Regulation of blood–brain barrier integrity and cognition by the microbiome-associated methylamines trimethylamine-*N*-oxide and trimethylamine

Lesley Hoyles[1]*, Matthew G. Pontifex[2], Ildefonso Rodriguez-Ramiro[2,3], M. Areeb Anis-Alavi[4], Tom Snelling[5], Egle Solito[6,7], Sonia Fonseca[8], Ana L. Carvalho[8], Simon R. Carding[2,8], Michael Müller[2], Robert C. Glen[5,9] David Vauzour[2] & Simon McArthur[4]*

[1]Department of Biosciences, School of Science and Technology, Nottingham Trent University, Clifton, Nottingham, UK

[2]Norwich Medical School, University of East Anglia, Norwich, UK

[3]Metabolic Syndrome Group, Madrid Institute for Advanced Studies (IMDEA) in Food, Madrid, E28049, Spain

[4]Institute of Dentistry, Barts & the London School of Medicine & Dentistry, Blizard Institute, Queen Mary University of London, London, UK

[5]Faculty of Medicine, Department of Metabolism, Digestion and Reproduction, Imperial College London, London, UK

[6]William Harvey Research Institute, Barts & the London School of Medicine & Dentistry, Queen Mary, University of London, London, UK

[7]Dipartimento di Medicina molecolare e Biotecnologie mediche, Federico II University, Naples, Italy

[8]The Gut Microbes and Health Research Programme, The Quadram Institute, Norwich Research Park, Norwich, UK

[9]Centre for Molecular Informatics, Department of Chemistry, University of Cambridge, Cambridge, UK

***Corresponding authors:** Lesley Hoyles, lesley.hoyles@ntu.ac.uk; Simon McArthur, s.mcarthur@qmul.ac.uk

Running title: Dietary methylamines affect the blood–brain barrier

Abbreviations: BBB, blood–brain barrier; DI, discrimination index; GO, gene ontology; KEGG, Kyoto Encyclopedia of Genes and Genomes; LPS, lipopolysaccharide; NOR, novel object recognition; SCFA, short-chain fatty acid; OFT, open field test; SPIA, signalling pathway impact analysis; TEER, transendothelial electrical resistance; TMA, trimethylamine; TMAO, trimethylamine *N*-oxide.

Supplementary materials associated with the article are available from figshare (https://doi.org/10.6084/m9.figshare.13549334.v1).

ABSTRACT

Communication between the gut microbiota and the brain is primarily mediated *via* soluble microbe-derived metabolites, but the details of this pathway remain poorly defined. Methylamines produced by microbial metabolism of dietary choline and L-carnitine have received attention due to their proposed association with vascular disease, but their effects upon the cerebrovascular circulation have not hitherto been studied. Here we use an integrated *in vitro*/*in vivo* approach to show that physiologically relevant concentrations of the dietary methylamine trimethylamine *N*-oxide (TMAO) enhanced and protected blood-brain barrier (BBB) integrity, acting through the tight junction regulator annexin A1. In contrast, the TMAO precursor trimethylamine (TMA) impaired BBB function and disrupted tight junction integrity. Moreover, we show that long-term exposure to TMAO has beneficial effects upon cognition in mice, improving visual recognition memory. Our findings demonstrate a direct interaction of microbiome-associated metabolites with the mammalian BBB, with consequences for cerebrovascular and cognitive function.

INTRODUCTION

As the role of the gut microbiota in host physiology and disease is categorised, novel pathways through which these interactions are mediated continue to emerge. We and others recently identified the blood–brain barrier (BBB) as a target for gut microbe-derived short-chain fatty acid (SCFA) activity, with butyrate and propionate acting to promote BBB integrity and protect the cerebral vasculature from insult[1,2]. SCFAs represent just one of many classes of gut microbe-derived metabolites, with little known as to how these other classes may influence BBB function.

Dietary methylamines, such as choline, phosphatidylcholine, betaine and trimethylamine-*N*-oxide (TMAO), are a class of metabolites receiving considerable attention as modulators of vascular function[3,4], although the mechanism(s) by which they affect human physiology remain poorly understood. The aforementioned methylamines can be broken down by members of the gut microbiota into trimethylamine (TMA)[5], which is carried from the gut through the portal vasculature to the liver and rapidly converted into TMAO by flavin monooxygenases[6]. TMAO then enters the systemic circulation, reaching fasting plasma concentrations of between 2 and 40 μM in humans[7–9], prior to excretion through the urine[5]. Approximately ten-fold lower concentrations of TMA compared with TMAO are found in the circulation under normal physiological conditions.

Early observational work reported an apparent association between atherosclerosis and elevated levels of TMAO[10,11]. Similarly, pre-clinical studies demonstrate the damaging effects of supraphysiological TMAO doses in atherosclerosis-prone mice[12] and upon thrombus formation[13]. Despite this, the impact of TMAO upon the vasculature remains uncertain, with a number of detailed studies encompassing both human and murine systems failing to replicate these initial findings[14], instead suggesting that this negative relationship disappears upon correction for renal function[4,15–17]. This indicates that the raised TMAO levels may in fact reflect impaired excretion rather than being a causative factor of disease. Moreover, protective roles for TMAO have been reported in rodent models of hypertension[18], atherosclerosis[19] and non-alcoholic steatohepatitis[20] and we have previously shown TMAO to improve glucose homeostasis and insulin secretion in mice fed a high-fat diet[21]. Perhaps helping to clarify this apparent contradiction, recent studies have established that

89 intravenous treatment of rats with the TMAO precursor TMA, but not TMAO itself,
90 increases mean arterial blood pressure[22]. Notably, the majority of reports describing
91 associations of plasma TMAO with cardiovascular disease have not concurrently
92 monitored levels of TMA; TMA but not TMAO has been shown to associate with severe
93 aortic stenosis[22] and gestational diabetes risk[23].
94
95 Beyond vascular health, dietary methylamines have implications for cognition, with a
96 positive correlation observed between choline intake and cognitive function in both
97 humans[24,25] and mice[26,27]. In contrast, cerebrospinal fluid TMAO levels have been
98 indicated as predictive of cognitive decline in Alzheimer's disease[28], while suppression
99 of microbial TMA/TMAO production improves cognitive function in the murine
100 APP/PS1 model of Alzheimer's disease[29]. Given the disparities in the literature
101 regarding the effects of methylamines upon the vasculature, and our increasing
102 awareness of the BBB as a major actor in the pathology of multiple neurological
103 conditions, we investigated the effects of physiologically relevant concentrations of
104 TMAO and its precursor TMA upon BBB integrity and cognitive behaviour.
105

106 **METHODS**

107

108 *Endothelial cell culture*

109 The human cerebromicrovascular endothelial cell line hCMEC/D3 was maintained and
110 treated as described previously[2,30]. Cells bearing shRNA sequences targeting annexin
111 A1 (*ANXA1*) or non-specific scramble sequences were produced as described
112 previously[31]; the degree of *ANXA1* knock-down was confirmed by flow cytometry
113 analysis (Suppl. Fig. 1). For all lines, cells were cultured to confluency in complete
114 EBM-2MV microvascular endothelial cell growth medium (Promocell GmbH,
115 Heidelberg, Germany), whereupon medium was replaced by EBM-2MV without VEGF
116 and cells were further cultured for a minimum of 4 days to enable intercellular tight
117 junction formation prior to experimentation.

118

119 *In vitro barrier function assessments*

120 Paracellular permeability and transendothelial electrical resistance (TEER) were
121 measured on 100 % confluent hCMEC/D3 cultures polarised by growth on 24-well
122 plate polyethylene terephthalate (PET) transwell inserts (surface area: 0.33 cm^2, pore
123 size: 0.4 µm; Greiner Bio-One GmbH, Kremsmünster, Austria) coated with calf-skin
124 collagen and fibronectin (Sigma-Aldrich, UK). The permeability of hCMEC/D3 cell
125 monolayers to 70 kDa FITC-dextran (2 mg/ml) was measured as described
126 previously[31–33]. TEER measurements were performed using a Millicell ERS-2
127 Voltohmmeter (Millipore, Watford, UK) and were expressed as $\Omega.cm^2$. In all cases,
128 values obtained from cell-free inserts similarly coated with collagen and fibronectin
129 were subtracted from the total values. In some cases, barrier integrity was tested by
130 challenge with bacterial lipopolysaccharide (LPS). Confluent hCMEC/D3 monolayers
131 were treated with TMAO or TMA for 12 h, whereupon LPS (*Escherichia coli* O111:B4;
132 50 ng/ml, comparable to circulating levels of LPS in human endotoxemia[34]) was added
133 for a further 12 h, without wash-out. Barrier function characteristics were then
134 interrogated as described above.

135

136 *Cell adhesion assays*

137 hCMEC/D3 cells were cultured to confluency on transwell inserts (0.4 µm pore size,
138 0.33 cm^2 diameter, Greiner Bio-One Gmbh, Austria) prior to 16 h treatment with 10
139 ng/ml TNFα. Monolayers were then incubated for 2 h with U937 monocytic cells pre-

140 labelled according to manufacturer's instructions with CMFDA cell tracker dye
141 (ThermoFisher Scientific, UK). Co-cultures were washed vigorously with ice-cold PBS
142 three times and fixed by incubation for 10 min in 1 % formaldehyde in 0.1 M PBS. Co-
143 cultures were mounted and examined using an Axiovert 200M inverted microscope
144 (Zeiss) equipped with a 20x objective lens. Images were captured with ZEN imaging
145 software (Carl Zeiss Ltd, UK) and analysed using ImageJ 1.53c (National Institutes of
146 Health, USA).
147
148 *Microarrays*
149 hCMEC/D3 cells were grown on 6-well plates coated with calf-skin collagen (Sigma-
150 Aldrich, Gillingham, UK), and collected in TRIzol (Thermo-Fisher Scientific, UK) as
151 described previously[2]. Total RNA was extracted using a TRIzol Plus RNA purification
152 kit (Thermo-Fisher Scientific, UK) and quantified using a CLARIOstar
153 spectrophotometer equipped with an LVis microplate (BMG Labtech GmbH,
154 Germany).
155
156 Hybridization experiments were performed by Macrogen Inc. (Seoul, Republic of
157 Korea) using Illumina HumanHT-12 v4.0 Expression BeadChips (Illumina Inc., San
158 Diego, CA) as described previously[2].
159
160 *Processing and analyses of array data*
161 Raw data supplied by Macrogen were quality-checked, $\log_2$-transformed and loess-
162 normalized (2 iterations) using affy[35]. Probe filtering and matching of probes not
163 classified as 'Bad' or 'No match' to Entrez identifiers were done as described
164 previously[2]. Average gene expression values were used for identification of
165 differentially expressed genes. Array data have been deposited in ArrayExpress under
166 accession number E-MTAB-6662. Normalized data are available (Supplementary
167 Table 1).
168
169 Enrichr[36,37] was used to perform Gene Ontology (GO) analysis. Signaling Pathway
170 Impact Analysis (SPIA) was used to determine whether Kyoto Encyclopedia of Genes
171 and Genomes (KEGG) pathways were activated or inhibited in hCMEC/D3 cells
172 exposed to TMAO or TMA[38]. Human KEGG pathways (KGML format) downloaded

173 from the KEGG PATHWAY database[39] were used for network (KEGGgraph, RBGL[40])
174 analysis.
175
176 *Immunofluorescence microscopy*
177 hCMEC/D3 cells were cultured on 24-well plate polyethylene terephthalate (PET)
178 transwell inserts (surface area: 0.33 cm^2, pore size: 0.4 µm; Greiner Bio-One GmbH,
179 Kremsmünster, Austria) coated with calf-skin collagen and fibronectin (Sigma-Aldrich,
180 UK), prior to immunostaining according to standard protocols[2,31] and using a primary
181 antibody directed against zonula occludens-1 (ZO-1; 1:100, ThermoFisher Scientific,
182 UK) or Alexafluor 488-conjugated phalloidin (1:140, ThermoFisher Scientific, UK).
183 Nuclei were counterstained with DAPI (Sigma-Aldrich, UK). Images were captured
184 using an LSM880 confocal laser scanning microscope (Carl Zeiss Ltd, Cambridge,
185 UK) fitted with 405 nm and 488 nm lasers, and a 63x oil immersion objective lens (NA,
186 1.4 mm, working distance, 0.17 mm). Images were captured with ZEN imaging
187 software (Carl Zeiss Ltd, UK) and analysed using ImageJ 1.53c (National Institutes of
188 Health, USA).
189
190 *Flow cytometry analysis*
191 Following experimental treatment, hCMEC/D3 cells were detached using 0.05%
192 trypsin and incubated with an unconjugated rabbit polyclonal antibody directed against
193 ANXA1 (1:1000, ThermoFisher Scientific, UK) on ice for 30 minutes, followed by
194 incubation with an AF488-conjugated goat anti-rabbit secondary antibody (1:500,
195 ThermoFisher Scientific, UK). Similarly detached hCMEC/D3 cells were incubated
196 with APC-conjugated mouse monoclonal anti-BCRP (1:100, BD Biosciences, Oxford,
197 UK), or PE-conjugated mouse monoclonal anti-MDR1A (1:100, BD Biosciences, UK)
198 antibodies on ice for 30 minutes, alongside fluorescence minus one controls.
199 Immunofluorescence was analysed for 20,000 events per treatment using a BD
200 FACSCanto II (BD Biosciences, UK) flow cytometer; data were analysed using FlowJo
201 8.0 software (Treestar Inc., CA, USA).
202
203 *Efflux transporter assays*
204 Activity of the major efflux transporters P-glycoprotein and BCRP was determined
205 through the use of commercially available assays (PREDEASY™ ATPase Assay Kits,
206 Solvo Biotechnology Inc., Budapest, Hungary), performed according to the

207 manufacturer's instructions. Stepwise dose–response curves centred around reported
208 physiological circulating concentrations of TMA (4.9 nM – 10.8 μM) and TMAO (0.5
209 μM – 1.08 mM) were constructed ($n = 4$) to investigate inhibitory effects of the
210 methylamines upon transporter activity.
211
212 *ELISA*
213 Culture medium ANXA1 content was assayed by specific ELISA as described
214 previously[41]. Serum TNFα and IL-1β concentrations were assayed using commercial
215 ELISA kits according to the manufacturer's instructions (ThermoFisher Scientific, UK).
216
217 *Animal experiments*
218 All animal experiments were performed according to the UK Animals (Scientific
219 Procedures) Act of 1986, under UK Home Office Project Licences PFA5C4F4F (short
220 term studies) and 70/8710 (long term studies), following ethical review by the Animal
221 Welfare and Ethical Review Boards of Queen Mary, University of London or the
222 University of East Anglia, respectively. Wild-type male C57Bl/6J mice (Charles River
223 Ltd., Harlow, UK) aged 8 weeks at the start of procedures were used throughout, with
224 a group size of n=6 for short term studies and n=8 for long-term/behavioural analyses.
225 Animals were housed in individually ventilated cages on a daily 12 h:12 h light/dark
226 cycle with, unless otherwise indicated, *ad libitum* access to standard mouse chow and
227 drinking water. Experimental procedures were started at 9 am to minimise variation
228 associated with circadian rhythms.
229
230 *Assessment of acute effects of TMAO on BBB integrity*
231 Mice (n=4-6 per group) were injected i.p. with 1.8 mg/kg body weight TMAO in 100 μl
232 saline vehicle, a dose calculated to approximate human circulating TMAO levels[42],
233 followed 2 h, 6 h or 24 h later by assessment of Evans blue extravasation as described
234 below. Alternatively, mice were injected i.p. with 3 mg/kg body weight LPS or 100 μl
235 0.9% saline vehicle, followed 2 h later by i.p. injection of either 1.8 mg/kg body weight
236 TMAO or 100 μl 0.9% saline vehicle for assessment of Evans blue extravasation 2 h
237 later. In both experiments, one hour before assessment animals were injected i.p. with
238 100 μl of a 2% (w/v) solution of Evans blue dye in 0.9 % saline (Sigma–Aldrich Ltd,
239 Poole, UK). Dye was permitted to circulate for 1 h before animals were transcardially

240 perfused with 0.9% saline at 4 °C to remove circulating dye. Brains were removed,
241 bisected and homogenized by maceration in 0.9% saline. Suspended macromolecules
242 were precipitated by incubation with 60% trichloroacetic acid, and dye content of
243 resulting supernatants was detected using a CLARIOstar spectrophotometer (BMG
244 Labtech GmbH, Germany) alongside a standard curve of defined concentrations of
245 Evans blue in the same buffer. Brain Evan's blue content was expressed as µg of dye
246 per mg of brain tissue, normalized to circulating plasma concentrations.
247
248 *Long-term LPS and TMAO treatments*
249 To assess the long-term impact of both LPS and TMAO on cognitive performance,
250 mice were divided into four groups (n=8 per group): 1) Water + PBS; 2) Water + TMAO;
251 3) LPS + PBS; 4) LPS + TMAO. C57Bl/6 mice were administered phosphate-buffered
252 saline (PBS) or LPS (*Escherichia coli* O55:B5, Sigma-Aldrich, UK) via intraperitoneal
253 (i.p.) injection (0.5 mg/kg/wk) for 8 weeks[43]. A final LPS treatment was administered
254 the day before sacrifice for nine total injections. Body weights were recorded prior to
255 each injection. TMAO was provided in the drinking water (500 mg/L) and water bottles
256 replaced every other day. Drinking volumes were recorded before bottle change.
257
258 *Processing and analyses of RNAseq data*
259 Mice were transcardially perfused with 0.9% saline at 4 °C to remove circulating blood,
260 and brains were removed and collected into RNAlater (Thermofisher Scientific Ltd.,
261 UK) prior to storage at -20 °C for later analysis. Whole brain total RNA was extracted
262 using a PureLink RNA Mini Kit (Thermofisher Scientific Ltd., UK) and quantified using
263 a CLARIOstar spectrophotometer equipped with an LVis microplate (BMG Labtech
264 GmbH, Germany). RNA samples (*n*=3 TMAO, *n*=3 control) were sent to Macrogen Inc.
265 (Republic of Korea) where they were subject to quality checks (RIN analysis); libraries
266 were prepared (TruSeq Stranded mRNA LT Sample Prep Kit) for paired-end (2x 100
267 nt) sequencing on an Illumina HiSeq 4000 apparatus. Raw RNAseq sequence data
268 (delivered in fastq format) were processed in house as follows. Reads were mapped
269 onto the mouse genome (mm10) using HISAT2 v2.1.0[44]. Number of reads in each
270 sample that mapped to genes in the BAM files returned by HISAT2 was determined
271 using featureCounts v1.6.4[45]. Entrez gene identifiers were converted to gene symbols
272 using *Mus musculus* annotations downloaded from NCBI on 26 November 2020; only
273 those genes with valid Entrez gene identifiers were retained in analyses. Raw RNAseq

274 data have been deposited with ArrayExpress under accession number E-MTAB-9869.
275 Significantly differentially expressed genes (P<0.1) were analysed by mouse KEGG
276 pathway over-representation analysis using Enrichr and manual curation.
277
278 *Behavioural analyses*
279 Behavioural tests were performed in the order they are introduced below. Apparatus
280 was cleaned using 70 % ethanol upon completion of each trial, eliminating any residual
281 odour.
282
283 Open field test (OFT) was conducted as previously described[46]. Briefly, mice were
284 placed in the centre of the OFT, a grey 50 x 50 x 50 cm apparatus illuminated with low
285 lux (100 lux) lighting. Total travel distance and time spent in the centre of the field was
286 determined at 5 min with a video tracking system (Smart 3.0 tracking software, Panlab,
287 Kent, UK).
288
289 The novel object recognition (NOR), a measure of recognition memory, was performed
290 as described previously[47,48], with slight modifications. Briefly, on day 1 mice were
291 habituated in a grey 50 x 50 x 50 cm apparatus illuminated with low lux (100 lux)
292 lighting, mice were placed into the empty maze and allowed to move freely for 10 min.
293 On day 2, mice were conditioned to a single object for a 10 min period. On day 3, mice
294 were placed into the same experimental area in the presence of two identical objects
295 for 15 min, after which they were returned to their respective cages and an inter-trial
296 interval of 1 h was observed. One familiar object was replaced with a novel object.
297 Mice were placed back within the testing area for a final 10 min. Videos were analysed
298 for a 5 min period, after which if an accumulative total of 15 s with both objects failed
299 to be reached, analysis continued for the full 10 min or until 15 s was achieved. Those
300 not achieving 15 s were excluded from the analysis[49]. A discrimination index (DI) was
301 calculated as follows: DI = (TN−TF)/(TN+TF), where TN is the time spent exploring
302 the novel object and TF is the time spent exploring the familiar object.
303
304 Y-maze spontaneous alternation test, a measure of spatial working memory, was
305 performed on the final day of behavioural testing as previously described[50]. Briefly, the
306 Y-maze apparatus comprised white Plexiglas (dimensions 38.5 × 8 × 13 cm, spaced
307 120° apart) and was illuminated with low lux (100 lux) lighting. Mice were placed in the

308 maze and allowed to explore freely for 7 min while tracking software recorded zone
309 transitioning and locomotor activity (Smart 3.0 tracking software, Panlab, Kent, UK).
310 Spontaneous alternation was calculated using the following formula: Spontaneous
311 Alternation = (Number of alternations/ Total Arm entries - 2) x 100.
312
313 *Extravasation assay and sample processing following long-term treatment*
314 Twenty-four hours after the final injection of LPS, mice were injected i.p. with 200 µl of
315 2% sodium fluorescein in sterile ddH_2O and anesthetized 30 min later with isoflurane
316 (1.5%) in a mixture of nitrous oxide (70%), and oxygen (30%). Once sedated, blood
317 was collected by cardiac puncture and centrifuged at 1,500 × g for 15 min at 4 °C to
318 collect the serum. The samples were analysed immediately for sodium fluorescein
319 extravasation or snap-frozen in liquid nitrogen and stored at -80 °C until further
320 analysis.
321
322 Mice were then transcardially perfused with saline containing 10 kU/ml heparin
323 (Sigma, Devon, UK). Dissected left hemi-brains were fixed in 4% PFA for 24 h and
324 embedded into paraffin before being processed for immunohistochemical analysis.
325 Right hemi-brains were stored at -80 °C until further analysis; cerebellums were
326 processed immediately for the sodium fluorescein extravasation assay. Cleared
327 volume of sodium fluorescein that passed from the plasma into the brain was
328 calculated as described previously[43].
329
330 *Statistical analyses*
331 Sample sizes were calculated to detect differences of 15 % or more with a power of
332 0.85 and α set at 5 %, calculations being informed by previously published data[2,31]. *In*
333 *vitro* experimental data (except those for *in vitro* microarray experiments) are
334 expressed as mean ± SEM, with a minimum of n = 3 independent experiments
335 performed in triplicate for all studies. In all cases, normality of distribution was
336 established using the Shapiro–Wilks test, followed by analysis with two-tailed
337 Student's *t*-tests to compare two groups or, for multiple comparison analysis, 1- or 2-
338 way ANOVA followed by Tukey's HSD *post hoc* test. Where data were not normally
339 distributed, non-parametric analysis was performed using the Wilcoxon signed rank
340 test. A P value of less than or equal to 5 % was considered significant. Differentially
341 expressed genes were identified in microarray data using LIMMA (Ritchie *et al*, 2015);

342 *P* values were corrected for multiple testing using the Benjamini–Hochberg procedure
343 (False Discovery Rate); a *P* value of less than or equal to 10 % was considered
344 significant in this case; *n* = 5 for control, TMAO and TMA groups. Significantly
345 differentially expressed genes (P_{FDR}<0.1) in RNAseq data (Supplementary Table 11)
346 were identified using DESeq2 v1.22.1[51].
347

348 **RESULTS**

349 To provide an initial assessment of the effects of the methylamines TMA and TMAO
350 upon the BBB we used a well-established *in vitro* BBB model, hCMEC/D3
351 immortalised human cerebromicrovascular cell monolayers grown under polarising
352 conditions on a Transwell filter, examining two key barrier properties: paracellular
353 permeability to a protein-sized tracer and TEER. Exposure of hCMEC/D3 cells for 24 h
354 to TMA (0-40 μM) caused a clear dose-dependent increase in paracellular
355 permeability to 70 kDa FITC-dextran (Fig. 1A), with normal circulating levels (0.4 μM)
356 of TMA and upwards significantly enhancing permeability. In contrast, exposure for
357 24 h to TMAO (0-4000 μM) caused a biphasic dose-dependent response (Fig. 1A),
358 with normal circulating concentrations (40 μM) significantly reducing permeability to
359 the tracer, an effect lost at 10-fold greater TMAO concentrations and reversed at 100-
360 fold greater TMAO (4 mM), where a significant increase in paracellular permeability
361 was apparent. In contrast, TMA had no effect upon TEER at any concentration studied,
362 while TMAO enhanced TEER by approximately 65%, an effect that was notably dose-
363 independent (Fig. 1B).

364

365 The physical barrier that the BBB provides is only one aspect by which it separates
366 the brain parenchymal environment from the periphery, equally important is the
367 immunological barrier that it represents. To model this, we employed a simple system
368 in which adhesion of CMFDA-labelled U937 monocytic cells to TNFα-activated
369 (10 ng/ml, 16 h) hCMEC/D3 monolayers was quantified in response to TMA or TMAO
370 treatment. Treatment with a physiologically relevant concentration of TMA (0.4 μM[42],
371 24 h post-TNFα) had no effect on the density of adherent U937 cells, but exposure of
372 hCMEC/D3 monolayers to physiological levels of TMAO (40 μM[42], 24 h post-TNFα)
373 significantly reduced U937 cell adhesion by approximately 50% compared to cultures
374 stimulated with TNFα alone (Fig. 1C).

375

376 The endothelial cells of the BBB express numerous efflux transporter proteins that
377 serve to limit entry of endogenous and exogenous molecules into the parenchyma,
378 with BCRP and P-glycoprotein being two of the most important. Consequently, we
379 examined whether treatment with TMA or TMAO affected function or expression of
380 either of these two transporters. Using commercially available *in vitro* assays, neither

381 methylamine affected BCRP or P-glycoprotein activity across a wide concentration
382 range (TMA: 4.9 nM to 10.8 μM; TMAO 0.5 μM to 1.08 mM) (Suppl. Fig. 2A-D).
383 Similarly, treatment of hCMEC/D3 cells for 24 h with physiologically relevant
384 concentrations of TMA (0.4 μM) or TMAO (40 μM) was without effect on cell surface
385 expression of either BCRP or P-glycoprotein (Suppl. Fig. 2E-F).
386
387 *Methylamine-induced changes in gene expression*
388 Having identified significant TMA-/TMAO-induced functional changes in endothelial
389 barrier characteristics *in vitro*, we undertook a microarray analysis of hCMEC/D3 cells
390 treated with either TMA (0.4 μM, 24 h) or TMAO (40 μM, 24 h) to investigate the
391 transcriptional changes underlying these effects. Treatment with TMA had a significant
392 (P_{FDR}<0.1) effect on 49 genes, with the expression of 39 upregulated and 10
393 downregulated (Fig 2A, Supplementary Table 2). In contrast, treatment with TMAO
394 had a significant (P_{FDR}<0.1) effect on 440 genes with 341 upregulated and 99
395 downregulated (Fig. 2B, Supplementary Table 3). *FMO3* gene expression was not
396 affected by TMA or TMAO at the physiological concentrations employed (Suppl. Fig.
397 3).
398
399 SPIA of the 440 TMAO-affected genes showed activation of the tight junction pathway
400 (P = 0.031), but significance was lost after correction for multiple testing
401 (Supplementary Table 4). No pathways were shown to be activated or inactivated by
402 the 49 TMA-affected genes (data not shown).
403
404 Gene ontology (GO) analysis was performed on TMA- and TMAO-regulated genes
405 using Enrichr[36,37]. TMA up-regulated and down-regulated genes were significantly
406 (P_{FDR}<0.2) associated with processes indicative of a degree of cellular stress (Fig 2C,
407 Supplementary Table 5, Supplementary Table 6). In contrast, genes up-regulated by
408 TMAO treatment were associated with regulation of the cytoskeleton and cell
409 morphology and with actin bundle formation (P_{FDR}<0.2), whereas pathways associated
410 with inflammatory signalling were down-regulated (Fig 2D, Supplementary Table 7,
411 Supplementary Table 8).
412
413 We then assessed the topology of a directional network of the 440 TMAO-associated
414 genes mapped onto all human KEGG pathways. In line with the GO analysis described

415 above, a number of genes of differing function were regulated by TMAO treatment,
416 with two principal groupings being particularly evident, namely those associated with
417 aspects of cellular metabolism and with regulation of actin cytoskeletal dynamics
418 (Figure 2E). Finally, we compared the 19,309 genes represented on the microarray
419 with a set of 203 genes[2] known to be associated with the BBB. While TMA treatment
420 had no significant effects on expression of these genes (Supplementary Table 9),
421 TMAO significantly (P_{FDR}<0.1) upregulated expression of four genes from this set
422 associated with transporter proteins and barrier integrity (Table 1, Supplementary
423 Table 10).
424
425
426 Given these transcriptional indications, and the fact that the restrictive properties of
427 the BBB are largely governed by inter-endothelial cell tight junctions linked *via* the
428 zonula occludens complex to the actin cytoskeleton[52], we hypothesised that TMA and
429 TMAO may affect barrier permeability through modification of the links between tight
430 junctions and the actin cytoskeleton. Confocal immunofluorescence microscopy of
431 hCMEC/D3 monolayers treated with a physiologically relevant concentration of TMA
432 (0.4 μM, 24 h) or TMAO (40 μM, 24 h) revealed clear changes to both ZO-1 and
433 fibrillar actin disposition within cells (Fig. 2F). Compared to untreated cells in which
434 both ZO-1 and F-actin fibres clearly defined the cellular perimeter, cells treated with
435 TMA exhibited a broken, patchy distribution of perimeter ZO-1 expression, and the
436 appearance of marked cytoplasmic F-actin stress fibres. In contrast, cells treated with
437 TMAO showed little change in ZO-1 distribution, but a marked enhancement of cortical
438 F-actin fibre thickness and intensity.
439
440 *The actions of TMAO are mediated through annexin A1 signalling*
441 Of the four BBB-associated genes identified as upregulated by TMAO, *ANXA1* is of
442 particular interest as we have previously shown this protein to regulate BBB tightness
443 *in vitro* and *in vivo* through modulation of the actin cytoskeleton[53]. Examination of
444 ANXA1 expression in hCMEC/D3 cells revealed that while total cellular levels of the
445 protein were not changed by either TMA (0.4 μM, 24 h) or TMAO (40 μM, 24 h)
446 treatment (Fig. 3A), TMA significantly suppressed and TMAO significantly augmented
447 medium ANXA1 content (Fig. 3B), a finding of interest given that autocrine/paracrine
448 effects are a major route of ANXA1 action[54].

449

450 To establish the importance of ANXA1 in mediating the effects of TMAO, we
451 investigated the effects of its depletion through use of hCMEC/D3 clones stably
452 transfected with shRNA sequences targeting *ANXA1* mRNA (Suppl. Fig. 1).
453 Suppression of *ANXA1* expression significantly inhibited the effects of TMAO (40 μM,
454 24 h) upon both paracellular permeability and TEER (Fig. 3C-D), an effect not seen in
455 cells bearing non-targeting scramble shRNA sequences. The actions of ANXA1 are
456 mediated to a large extent through the G protein-coupled receptor formyl peptide
457 receptor 2 (FPR2)[55]. Hence, we investigated how inclusion of a well-characterised
458 antagonist to this receptor, WRW_4 (10 μM, 10 min pre-treatment), would affect the
459 functional response to TMAO. Pre-treatment with WRW_4 was able to significantly
460 attenuate the effects of TMAO treatment on both TEER (Fig. 3E) and paracellular
461 permeability (Fig. 3F), further indicating the role of ANXA1 signalling as the principal
462 mediator of TMAO actions on hCMEC/D3 cells.
463

464 *Acute beneficial effects of TMAO treatment in vivo*

465 While hCMEC/D3 endothelial cells are a widely used and generally representative
466 model, they cannot reflect all aspects of the multicellular neurovascular unit that
467 underlies BBB function, hence we investigated whether the beneficial effects of TMAO
468 identified *in vitro* translate to an *in vivo* situation. Initial studies revealed that systemic
469 administration of TMAO to wild-type male mice (1.8 mg/kg, i.p.) induced a time-
470 dependent reduction in BBB permeability to the tracer Evans blue (2 % in saline, 100
471 μl, i.p.), with a significant reduction in dye extravasation to the brain parenchyma being
472 apparent 2 h following TMAO administration, an effect lost at longer time-points (Fig.
473 4A), presumably due to the relatively short plasma half-life of TMAO *in vivo*[56]. To
474 further investigate this effect of TMAO, we employed a simple model of enhanced BBB
475 permeability, namely acute peripheral administration of bacterial LPS[31]. Treatment
476 with LPS (*E. coli* O111:B4, 3 mg/kg, i.p.) significantly enhanced intraparenchymal
477 extravasation of Evans blue within 4 h, an effect significantly attenuated by subsequent
478 treatment with TMAO (1.8 mg/kg, i.p.) 2 h post-LPS (Fig. 4B), further confirming a
479 beneficial action of TMAO at physiological concentrations upon the BBB *in vivo*.
480

481 *TMAO treatment rapidly alters brain transcriptional activity*

482 To investigate the wider actions of TMAO upon the brain we performed whole brain
483 RNAseq transcriptomic analysis of wild-type male mice 2 h following TMAO
484 administration (1.8 mg/kg i.p.). We identified 76 significantly differentially expressed
485 genes (P_{FDR}<0.1), with expression of 41 upregulated and 35 downregulated (Figure
486 5A; Supplementary Table 11). KEGG pathway analysis using Enrichr identified a
487 number of significantly regulated murine pathways (Figure 5B), including oxidative
488 phosphorylation, Parkinson's disease and Alzheimer's disease. Closer analysis of
489 regulated genes identified a number of general groupings (Figure 5C), with
490 downregulated genes associated with the mitochondrial respiratory chain (*COX1*,
491 *COX3*, *ATP6*, *ND4L*, *CYTB*, *ND1*, *ND3*, *ND4*, *ND6*) and ribosomal function (*mt-Rnr2*,
492 *mt-Rnr1*, *Rps23rg1*) and upregulated genes associated with cellular or axonal growth
493 (*Nme7*, *B3gat2*, *Fuz*, *Nefm*, *Basp1*, *Mtg1*, *Vps37a*, *Smim1*, *Araf*). Of the 203 BBB-
494 associated human genes previously identified[2], 197 had matches in our mouse brain
495 data set. Here, two genes were identified as significantly differentially expressed at
496 P_{FDR}<0.1: reduced *Cpe* (carboxypeptidase E) and increased *App* (amyloid precursor
497 protein) expression (Figure 5D; Supplementary Table 12).
498
499 *Chronic low-dose TMAO treatment prevents LPS-induced BBB disruption and*
500 *memory impairment*
501 The fundamental role of the BBB is to protect the brain, preserving its homeostatic
502 environment; damage to BBB integrity is therefore detrimental, and is believed to
503 directly contribute towards cognitive impairment[57–59]. Having shown TMAO to exert a
504 protective effect upon BBB function/integrity in response to acute inflammatory insult,
505 we next examined whether a similar effect held true for chronic conditions, and
506 whether this protection extended to cognition. TMAO was administered to male
507 C57Bl/6J mice through drinking water (0.5 mg/ml) over 2 months, in combination with
508 chronic low-dose LPS administration (0.5 mg/kg/week, i.p.) to model a mild
509 inflammatory stress known to impact cognitive behaviour[43]. There were no differences
510 in volumes of water drunk or, where relevant, final consumption of TMAO between any
511 groups (Table 2). The serum inflammatory cytokines TNFα and IL-1β were both
512 nominally elevated in response to LPS treatment, although not reaching statistical
513 significance, indicating a sub-clinical inflammatory response; TMAO had no effect on
514 TNFα nor IL-1β levels (Suppl. Fig. 4). Notably, animals exposed to LPS exhibited a

515 significant reduction in body weight gain compared to their untreated counterparts, an
516 effect reversed by TMAO treatment (Fig. 6A). Treatment with LPS increased
517 cerebellar FITC extravasation, an effect that was prevented by TMAO treatment,
518 although this did not reach statistical significance on *post hoc* analysis (Fig. 6B). To
519 corroborate these findings, we investigated a second marker of impaired BBB integrity,
520 confocal microscopic detection of brain perivascular IgG deposition. In comparison
521 with sham-treated animals, exposure to LPS caused a significant accumulation of IgG
522 in the perivascular compartment, an effect prevented by TMAO treatment (Fig. 6C).
523
524 The OFT confirmed neither LPS nor TMAO treatment affected motor function, with
525 movement speed and distance travelled comparable across treatment groups (Fig.
526 6D-E). Similarly, no effect was apparent on the proportion of time animals spent in the
527 centre of the field, suggesting limited effects upon anxiety (Fig. 6F). Working memory,
528 however, determined via NOR indicated a significant reduction in performance in
529 animals exposed to LPS, a behavioural deficit notably prevented in animals co-treated
530 with TMAO (Fig. 6G). In contrast, no effect of either LPS or TMAO treatment was
531 apparent in the Y-maze spontaneous alternation task (Fig. 6H) or in distance travelled
532 during this task (Fig. 6I), indicating no differences in spatial memory.
533
534

535 **DISCUSSION**

536

537 The relationship between the BBB and cognitive behaviour is complex and far from
538 being fully understood, but it is clear from both human and animal studies that deficits
539 in barrier integrity can exert a profound and deleterious effect upon memory, language
540 and executive function[60–63]. Indeed, BBB impairment is among the first events to occur
541 in the course of Alzheimer's disease, and may aggravate the pathological processes
542 that underlie the condition[64]. Strategies to promote BBB function may thus have
543 significant value in helping to protect the brain from progressive neurological diseases
544 such as dementia. In this study we identify novel and distinct roles for the microbiome-
545 associated dietary methylamines TMA and TMAO in regulating BBB function *in vitro*
546 and *in vivo* and provide evidence that the beneficial action of TMAO upon the BBB
547 coincides with similar protective effects upon cognition. These data reinforce the
548 position of the cerebral vasculature as a major target for the gut-brain axis, and extend
549 our knowledge of its interactions with microbial metabolites beyond SCFAs[1,2] to
550 another major class of molecules, the dietary methylamines.

551

552 Notably, our data show that while both TMA and TMAO have activity upon the
553 endothelium, there is a marked distinction between their effects despite their close
554 structural similarity. TMA, the direct product of microbial choline, L-carnitine and
555 TMAO metabolism in the upper gut[5], had a deleterious effect upon the endothelium,
556 disrupting cytoskeletal arrangement, inducing signs of metabolic stress and ultimately
557 impairing endothelial barrier integrity. In contrast, TMAO, largely derived from hepatic
558 FMO3-mediated oxidation of TMA taken up from the gut via the hepatic portal vein[6],
559 was beneficial for cerebral vascular integrity *in vitro* and *in vivo*. These differences
560 suggest that host conversion of TMA (a gas) to TMAO (a stable metabolite) may be
561 an effective detoxification pathway, emphasising the importance of host metabolic
562 pathways in modulating communication in the gut-brain axis, and underlining the
563 importance of using a systems-level approach to understand the interactions between
564 the host and its resident microbiota.

565

566 *TMAO and cognitive function*

567 Numerous groups have investigated the putative relationship between TMAO and
568 cognition following reports of an association between cerebrospinal fluid TMAO

content and Alzheimer's disease[28], with negative correlations between plasma TMAO content and cognitive function having been identified in both clinical[65–67] and experimental[29,68,69] settings. Whether this relationship is truly deterministic remains unclear, however, as the role of the immediate precursor to TMAO, TMA, in cognition and vascular function has largely been overlooked. This omission may be important in light of studies reporting negative correlations between cognitive impairment and serum TMA[70–72] and our own data showing a potent detrimental effect of physiological levels of TMA upon the cerebrovascular endothelium *in vitro*. Given that TMA has been shown to be detrimental in contexts other than cognitive function[22,23], the contribution that this metabolite plays in disease is evidently in need of closer attention.

Interpreting associations between circulating TMAO and cognition is further complicated by studies indicating that consumption of the TMAO precursors choline and L-carnitine can improve cognitive function[24,25,73], evidence that patients with Parkinson's disease have lower circulating TMAO than healthy controls[74], and more recent Mendelian randomisation analysis indicating that serum TMAO and Alzheimer's disease are not causally related[75]. Given this background, our data indicating that physiologically relevant concentrations of TMAO have positive effects upon both BBB integrity and cognition *in vivo* thus serve as a useful counterweight to population-level correlation studies. Interestingly, a number of previous interventional studies have been performed in mice, suggesting that substantially higher doses of TMAO may have detrimental effects upon learning and memory[68,69,76], although as we and others[77] have identified dose-dependency in the effects of TMAO *in vitro*, it seems plausible that this may reflect a similar phenomenon *in vivo*. The importance of investigating the impact of TMAO under physiologically relevant conditions is further emphasised by a recent study showing TMAO treatment to impair novel object recognition in mice[65], ostensibly an opposite finding to our data achieved with a similar dosing regimen. Importantly, however, mice in this study were maintained on a reduced choline diet, a condition known to alter hepatic metabolism[78]; what impact such changes might have on handling of (TMA and) TMAO by the body is unknown. These discrepancies may be instructive in guarding against incautious extrapolation of TMAO effects from healthy to diseased populations.

Could TMAO contribute to the beneficial effects of a seafood-rich diet?

603 Consumption of a diet rich in fish and other seafood, known to provide significant
604 quantities of TMAO[79], associates with a reduced risk of cognitive decline[80,81] and
605 protection against cerebrovascular disease[82]. These effects have in large part been
606 attributed to beneficial actions of the omega-3 polyunsaturated fatty acids[83], although
607 there is little evidence that their direct supplementation improves cognitive function[84]
608 or stroke risk[85]. Here we provide evidence that another component of a seafood-rich
609 diet, TMAO, has protective effects on the cerebral vasculature and upon cognition,
610 indicating that broadening the scope of nutritional analyses beyond the omega-3 fatty
611 acids may be worthwhile. In particular, we demonstrate that TMAO acts to stimulate
612 endothelial secretion of a major regulator of BBB permeability, ANXA1[53], leading *via*
613 autocrine/paracrine activation of its receptor FPR2 to cytoskeletal actin rearrangement
614 and enhanced BBB integrity.
615
616 This novel interaction between TMAO and ANXA1 may have implications beyond BBB
617 integrity, given that ANXA1 is a major mediator of inflammatory resolution[86], and
618 highlighted by our finding that TMAO treatment inhibited model immune cell adhesion
619 to activated endothelia *in vitro*. As with the link between a seafood-rich diet and
620 cerebrovascular health, fish consumption has been associated with reduced
621 inflammatory disease, again attributed primarily to a role for omega-3 fatty acids[87].
622 While it is too early to definitively claim an anti-inflammatory role for dietary
623 methylamines, particularly given the opposing actions of TMA and TMAO, our data do
624 suggest that investigation of the bioactive properties of seafood-rich diets should
625 progress beyond omega-3 fatty acids to focus on other potential contributors.
626
627 *Conclusions*
628 Interest in the role played by the gut microbiota in communication through the gut-
629 brain axis has grown dramatically in the last few years, with much attention focused
630 on the mediating actions of microbe-derived metabolites[88]. While a number of studies
631 have shown patterns in microbial metabolite production that associate with different
632 brain functions[89], detailed understanding of the role of individual molecules remains in
633 its infancy, with defined roles characterised for only a subset of the many molecules
634 known to be released by gut microbes. Here we show that the dietary methylamine
635 TMAO can beneficially modulate both BBB integrity and cognitive function *in vivo*,
636 providing direct mechanistic evidence for a positive role of this microbiome-associated

637 metabolite, and reinforce the position of the BBB as an interface in the gut-brain axis.
638 Notably, the positive effects of TMAO that we report stand in contrast to previous work
639 describing deleterious effects of TMAO exposure at high concentrations or under non-
640 physiological conditions[77], emphasising the importance of taking a holistic approach
641 to understanding gut microbiota-host interactions.
642
643

644 **COMPETING INTERESTS**

645 The authors declare that they have no competing interests.

646

647 **ACKNOWLEDGEMENTS**

648 This work was funded by Alzheimer's Research UK Pilot Grant No. ARUK-PPG2016B-
649 6. PREDEASY™ efflux transporter analysis kits were generously provided through the
650 SOLVO Biotechnology Research and Academic Collaborative Transporter Studies
651 (ReACTS) Program. This work used the computing resources of the UK MEDical
652 BIOinformatics partnership – aggregation, integration, visualisation and analysis of
653 large, complex data (UK MED-BIO), which was supported by the Medical Research
654 Council (grant number MR/L01632X/1). SF was supported by Fundación Alfonso
655 Martín Escudero. TS was supported by a bursary from the Imperial College London
656 Undergraduate Research Opportunities Programme. LH, DV and SM designed the
657 experiments. SM performed cellular assays and acute *in vivo* analyses. TS carried out
658 the initial permeability and TEER assays. MAA performed IgG extravasation studies.
659 ES produced and provided shRNA treated hCMEC/D3 clones. LH undertook all
660 processing and analyses of transcriptomic data. RCG provided valuable insight and
661 advice throughout the project. DV, MP, IR and MM performed the chronic *in vivo* LPS
662 challenge study and undertook all analyses of behavioural data. SRC, ALC and SF
663 contributed to preliminary animal work. LH, DV and SM wrote the manuscript. All
664 authors read and approved the final version of the manuscript.

665

666

667

668 **REFERENCES**

669 1. Braniste, V. *et al.* The gut microbiota influences blood-brain barrier permeability in
670 mice. *Sci. Transl. Med.* **6**, 263ra158-263ra158 (2014).
671 2. Hoyles, L. *et al.* Microbiome–host systems interactions: protective effects of
672 propionate upon the blood–brain barrier. *Microbiome 2018 61* **6**, 55–55 (2018).
673 3. Tang, W. H. W. & Hazen, S. L. Microbiome, trimethylamine N-oxide, and
674 cardiometabolic disease. *Transl. Res. J. Lab. Clin. Med.* **179**, 108–115 (2017).
675 4. Dinicolantonio, J. J., McCarty, M. & Okeefe, J. Association of moderately elevated
676 trimethylamine N-oxide with cardiovascular risk: Is TMAO serving as a marker for
677 hepatic insulin resistance. *Open Heart* **6**, e000890–e000890 (2019).
678 5. Hoyles, L. *et al.* Metabolic retroconversion of trimethylamine N-oxide and the gut
679 microbiota. *Microbiome* **6**, 73–73 (2018).
680 6. Zeisel, S. H., Wishnok, J. S. & Blusztajn, J. K. Formation of methylamines from
681 ingested choline and lecithin. *J. Pharmacol. Exp. Ther.* **225**, 320–324 (1983).
682 7. Kühn, T. *et al.* Intra-individual variation of plasma trimethylamine-N-oxide (TMAO),
683 betaine and choline over 1 year. *Clin. Chem. Lab. Med. CCLM* **55**, 261–268 (2017).
684 8. Duranton, F. *et al.* Normal and pathologic concentrations of uremic toxins. *J. Am.*
685 *Soc. Nephrol. JASN* **23**, 1258–70 (2012).
686 9. Bain, M., Faull, R., Fornasini, G., Milne, R. & Evans, A. Accumulation of
687 Trimethylamine and trimethylamine-N-oxide in End-Stage Renal Disease Patients
688 Undergoing Haemodialysis. *Nephrol. Dial. Transplant. Off. Publ. Eur. Dial. Transpl.*
689 *Assoc. - Eur. Ren. Assoc.* **21**, 1300–4 (2006).
690 10. Tang, W. H. W. *et al.* Intestinal microbial metabolism of phosphatidylcholine and
691 cardiovascular risk. *N. Engl. J. Med.* **368**, 1575–1584 (2013).
692 11. Tang, W. H. W. *et al.* Prognostic value of elevated levels of intestinal microbe-
693 generated metabolite trimethylamine-N-oxide in patients with heart failure: refining
694 the gut hypothesis. *J. Am. Coll. Cardiol.* **64**, 1908–1914 (2014).
695 12. Wang, Z. *et al.* Non-lethal Inhibition of Gut Microbial Trimethylamine Production for
696 the Treatment of Atherosclerosis. *Cell* **163**, 1585–1595 (2015).
697 13. Zhu, W. *et al.* Gut Microbial Metabolite TMAO Enhances Platelet Hyperreactivity
698 and Thrombosis Risk. *Cell* **165**, 111–124 (2016).
699 14. Aldana-Hernández, P. *et al.* Dietary Choline or Trimethylamine N-oxide
700 Supplementation Does Not Influence Atherosclerosis Development in Ldlr−/− and
701 Apoe−/− Male Mice. *J. Nutr.* (2019) doi:10.1093/jn/nxz214.

15. Miller, C. A. *et al.* Effect of egg ingestion on trimethylamine-N-oxide production in humans: a randomized, controlled, dose-response study. *Am. J. Clin. Nutr.* **100**, 778–786 (2014).
16. Jia, J. *et al.* Assessment of Causal Direction Between Gut Microbiota-Dependent Metabolites and Cardiometabolic Health: Abi-Directional Mendelian Randomisation Analysis. *Diabetes* (2019) doi:10.2337/db19-0153.
17. Winther, S. A. *et al.* Utility of Plasma Concentration of Trimethylamine N-Oxide in Predicting Cardiovascular and Renal Complications in Individuals With Type 1 Diabetes. *Diabetes Care* **42**, 1512–1520 (2019).
18. Huc, T. *et al.* Chronic, low-dose TMAO treatment reduces diastolic dysfunction and heart fibrosis in hypertensive rats. *Am. J. Physiol.-Heart Circ. Physiol.* **315**, H1805–H1820 (2018).
19. Collins, H. L. *et al.* L-Carnitine intake and high trimethylamine N-oxide plasma levels correlate with low aortic lesions in ApoE−/− transgenic mice expressing CETP. *Atherosclerosis* **244**, 29–37 (2016).
20. Zhao, Z.-H. *et al.* Trimethylamine N-oxide attenuates high-fat high-cholesterol diet-induced steatohepatitis by reducing hepatic cholesterol overload in rats. *World J. Gastroenterol.* **25**, 2450–2462 (2019).
21. Dumas, M.-E. *et al.* Microbial-Host Co-metabolites Are Prodromal Markers Predicting Phenotypic Heterogeneity in Behavior, Obesity, and Impaired Glucose Tolerance. *Cell Rep.* **20**, 136–148 (2017).
22. Jaworska, K., Bielinska, K., Gawrys-Kopczynska, M. & Ufnal, M. TMA (trimethylamine), but not its oxide TMAO (trimethylamine-oxide), exerts haemodynamic effects: implications for interpretation of cardiovascular actions of gut microbiome. *Cardiovasc. Res.* **115**, 1948–1949 (2019).
23. Huo, X. *et al.* Trimethylamine N-Oxide Metabolites in Early Pregnancy and Risk of Gestational Diabetes: A Nested Case-Control Study. *J. Clin. Endocrinol. Metab.* **104**, 5529–5539 (2019).
24. Poly, C. *et al.* The relation of dietary choline to cognitive performance and white-matter hyperintensity in the Framingham Offspring Cohort. *Am. J. Clin. Nutr.* **94**, 1584–1591 (2011).
25. Nurk, E. *et al.* Plasma free choline, betaine and cognitive performance: the Hordaland Health Study. *Br. J. Nutr.* **109**, 511–519 (2013).

735 26. Leathwood, P. D., Heck, E. & Mauron, J. Phosphatidyl choline and avoidance
736 performance in 17 month-old SEC/1ReJ mice. *Life Sci.* **30**, 1065–1071 (1982).
737 27. Bartus, R. T., Dean, R. L., Goas, J. A. & Lippa, A. S. Age-related changes in passive
738 avoidance retention: modulation with dietary choline. *Science* **209**, 301–3 (1980).
739 28. Vogt, N. M. *et al.* The gut microbiota-derived metabolite trimethylamine N-oxide is
740 elevated in Alzheimer's disease. *Alzheimers Res. Ther.* **10**, 124–124 (2018).
741 29. Gao, Q. *et al.* Decreased levels of circulating trimethylamine N-oxide alleviate
742 cognitive and pathological deterioration in transgenic mice: A potential therapeutic
743 approach for Alzheimer's disease. *Aging* **11**, 8642–8663 (2019).
744 30. Weksler, B. B. *et al.* Blood-brain barrier-specific properties of a human adult brain
745 endothelial cell line. *FASEB J. Off. Publ. Fed. Am. Soc. Exp. Biol.* **19**, 1872–4
746 (2005).
747 31. Maggioli, E. *et al.* Estrogen protects the blood-brain barrier from inflammation-
748 induced disruption and increased lymphocyte trafficking. *Brain. Behav. Immun.* **51**,
749 212–222 (2015).
750 32. Abbott, N. J., Hughes, C. C., Revest, P. A. & Greenwood, J. Development and
751 characterisation of a rat brain capillary endothelial culture: towards an in vitro
752 blood-brain barrier. *J. Cell Sci.* **103 (Pt 1**, 23–37 (1992).
753 33. Coisne, C. *et al.* Mouse syngenic in vitro blood-brain barrier model: a new tool to
754 examine inflammatory events in cerebral endothelium. *Lab. Investig. J. Tech.*
755 *Methods Pathol.* **85**, 734–46 (2005).
756 34. Pais de Barros, J.-P. *et al.* Quantitative lipopolysaccharide analysis using
757 HPLC/MS/MS and its combination with the limulus amebocyte lysate assay. *J.*
758 *Lipid Res.* **56**, 1363–9 (2015).
759 35. Gautier, L., Cope, L., Bolstad, B. M. & Irizarry, R. A. affy--analysis of Affymetrix
760 GeneChip data at the probe level. *Bioinforma. Oxf. Engl.* **20**, 307–15 (2004).
761 36. Chen, E. Y. *et al.* Enrichr: interactive and collaborative HTML5 gene list enrichment
762 analysis tool. *BMC Bioinformatics* **14**, 128–128 (2013).
763 37. Kuleshov, M. V. *et al.* Enrichr: a comprehensive gene set enrichment analysis web
764 server 2016 update. *Nucleic Acids Res.* **44**, W90-7 (2016).
765 38. Tarca, A. L. *et al.* A novel signaling pathway impact analysis. *Bioinforma. Oxf. Engl.*
766 **25**, 75–82 (2009).
767 39. Hoyles, L. *et al.* Molecular phenomics and metagenomics of hepatic steatosis in
768 non-diabetic obese women. *Nat. Med.* **24**, 1070–1080 (2018).

769 40. Zhang, J. D. & Wiemann, S. KEGGgraph: a graph approach to KEGG PATHWAY
770 in R and bioconductor. *Bioinforma. Oxf. Engl.* **25**, 1470–1471 (2009).
771 41. McArthur, S. *et al.* Annexin A1: a central player in the anti-inflammatory and
772 neuroprotective role of microglia. *J Immunol* **185**, 6317–6328 (2010).
773 42. Wishart, D. S. *et al.* HMDB 4.0: the human metabolome database for 2018. *Nucleic*
774 *Acids Res.* **46**, D608–D617 (2018).
775 43. Marottoli, F. M. *et al.* Peripheral Inflammation, Apolipoprotein E4, and Amyloid-β
776 Interact to Induce Cognitive and Cerebrovascular Dysfunction: *ASN Neuro* (2017)
777 doi:10.1177/1759091417719201.
778 44. Kim, D., Langmead, B. & Salzberg, S. L. HISAT: a fast spliced aligner with low
779 memory requirements. *Nat. Methods* **12**, 357–360 (2015).
780 45. Liao, Y., Smyth, G. K. & Shi, W. featureCounts: an efficient general purpose
781 program for assigning sequence reads to genomic features. *Bioinforma. Oxf. Engl.*
782 **30**, 923–930 (2014).
783 46. Hölter, S. M. *et al.* Tests for Anxiety-Related Behavior in Mice. *Curr. Protoc. Mouse*
784 *Biol.* **5**, 291–309 (2015).
785 47. Davis, K. E., Eacott, M. J., Easton, A. & Gigg, J. Episodic-like memory is sensitive
786 to both Alzheimer's-like pathological accumulation and normal ageing processes
787 in mice. *Behav. Brain Res.* **254**, 73–82 (2013).
788 48. Leger, M. *et al.* Object recognition test in mice. *Nat. Protoc.* **8**, 2531–2537 (2013).
789 49. Denninger, J. K., Smith, B. M. & Kirby, E. D. Novel Object Recognition and Object
790 Location Behavioral Testing in Mice on a Budget. *J. Vis. Exp. JoVE* (2018)
791 doi:10.3791/58593.
792 50. Thomas, R., Morris, A. W. J. & Tai, L. M. Epidermal growth factor prevents APOE4-
793 induced cognitive and cerebrovascular deficits in female mice. *Heliyon* **3**, e00319
794 (2017).
795 51. Love, M. I., Huber, W. & Anders, S. Moderated estimation of fold change and
796 dispersion for RNA-seq data with DESeq2. *Genome Biol.* **15**, 550 (2014).
797 52. Lochhead, J. J., Yang, J., Ronaldson, P. T. & Davis, T. P. Structure, Function, and
798 Regulation of the Blood-Brain Barrier Tight Junction in Central Nervous System
799 Disorders. *Front. Physiol.* **11**, 914 (2020).
800 53. Cristante, E. *et al.* Identification of an essential endogenous regulator of blood-
801 brain barrier integrity, and its pathological and therapeutic implications. *Proc. Natl.*
802 *Acad. Sci. U. S. A.* **110**, 832–841 (2013).

803 54. McArthur, S. *et al.* Annexin A1 regulates hormone exocytosis through a mechanism
804 involving actin reorganization. *FASEB J* **23**, 4000–4010 (2009).
805 55. Bena, S., Brancaleone, V., Wang, J. M., Perretti, M. & Flower, R. J. Annexin A1
806 interaction with the FPR2/ALX receptor: identification of distinct domains and
807 downstream associated signaling. *J. Biol. Chem.* **287**, 24690–7 (2012).
808 56. Cho, C. E. *et al.* Trimethylamine-N-oxide (TMAO) response to animal source foods
809 varies among healthy young men and is influenced by their gut microbiota
810 composition: A randomized controlled trial. *Mol. Nutr. Food Res.* **61**, 1600324
811 (2017).
812 57. Montagne, A. *et al.* Blood-Brain Barrier Breakdown in the Aging Human
813 Hippocampus. *Neuron* **85**, 296–302 (2015).
814 58. Taheri, S. *et al.* Blood-brain barrier permeability abnormalities in vascular cognitive
815 impairment. *Stroke J. Cereb. Circ.* **42**, 2158–63 (2011).
816 59. Bowman, G. L. *et al.* Blood-brain barrier impairment in Alzheimer disease: stability
817 and functional significance. *Neurology* **68**, 1809–14 (2007).
818 60. Merino, J. G. *et al.* Blood-brain barrier disruption after cardiac surgery. *AJNR Am.*
819 *J. Neuroradiol.* **34**, 518–523 (2013).
820 61. Hu, N. *et al.* Involvement of the blood-brain barrier opening in cognitive decline in
821 aged rats following orthopedic surgery and high concentration of sevoflurane
822 inhalation. *Brain Res.* **1551**, 13–24 (2014).
823 62. Abrahamov, D. *et al.* Blood-Brain Barrier Disruption After Cardiopulmonary
824 Bypass: Diagnosis and Correlation to Cognition. *Ann. Thorac. Surg.* **104**, 161–169
825 (2017).
826 63. Yang, S. *et al.* Anesthesia and Surgery Impair Blood-Brain Barrier and Cognitive
827 Function in Mice. *Front. Immunol.* **8**, 902–902 (2017).
828 64. Zenaro, E., Piacentino, G. & Constantin, G. The blood-brain barrier in Alzheimer's
829 disease. *Neurobiol. Dis.* (2016) doi:10.1016/j.nbd.2016.07.007.
830 65. Brunt, V. E. *et al.* The gut microbiome–derived metabolite trimethylamine N-oxide
831 modulates neuroinflammation and cognitive function with aging. *GeroScience*
832 (2020) doi:10.1007/s11357-020-00257-2.
833 66. He, W. *et al.* Trimethylamine N-Oxide, a Gut Microbiota-Dependent Metabolite, is
834 Associated with Frailty in Older Adults with Cardiovascular Disease. *Clin. Interv.*
835 *Aging* **15**, 1809–1820 (2020).

836 67. Zhu, C. *et al.* Association of plasma trimethylamine-N-oxide levels with post-stroke
837 cognitive impairment: a 1-year longitudinal study. *Neurol. Sci. Off. J. Ital. Neurol.*
838 *Soc. Ital. Soc. Clin. Neurophysiol.* **41**, 57–63 (2020).
839 68. Zhao, L. *et al.* Higher Circulating Trimethylamine N-oxide Sensitizes Sevoflurane-
840 Induced Cognitive Dysfunction in Aged Rats Probably by Downregulating
841 Hippocampal Methionine Sulfoxide Reductase A. *Neurochem. Res.* **44**, 2506–
842 2516 (2019).
843 69. Meng, F., Li, N., Li, D., Song, B. & Li, L. The presence of elevated circulating
844 trimethylamine N-oxide exaggerates postoperative cognitive dysfunction in aged
845 rats. *Behav. Brain Res.* **368**, 111902–111902 (2019).
846 70. Sanguinetti, E. *et al.* Microbiome-metabolome signatures in mice genetically prone
847 to develop dementia, fed a normal or fatty diet. *Sci. Rep.* **8**, (2018).
848 71. Liu, J. *et al.* Baicalin ameliorates neuropathology in repeated cerebral ischemia-
849 reperfusion injury model mice by remodeling the gut microbiota. *Aging* **12**, 3791–
850 3806 (2020).
851 72. Wang, Q.-J. *et al.* Concomitant memantine and Lactobacillus plantarum treatment
852 attenuates cognitive impairments in APP/PS1 mice. *Aging* **12**, 628–649 (2020).
853 73. Sawicka, A. K., Renzi, G. & Olek, R. A. The bright and the dark sides of L-carnitine
854 supplementation: a systematic review. *J. Int. Soc. Sports Nutr.* **17**, 49 (2020).
855 74. Chung, S. J. *et al.* Gut microbiota-derived metabolite trimethylamine N-oxide as a
856 biomarker in early Parkinson's disease. *Nutr. Burbank Los Angel. Cty. Calif* **83**,
857 111090 (2020).
858 75. Zhuang, Z. *et al.* Causal relationships between gut metabolites and Alzheimer's
859 disease: a bidirectional Mendelian randomization study. *Neurobiol. Aging* (2020)
860 doi:10.1016/j.neurobiolaging.2020.10.022.
861 76. Li, D. *et al.* Trimethylamine-N-oxide promotes brain aging and cognitive impairment
862 in mice. *Aging Cell* **17**, (2018).
863 77. Papandreou, C., Moré, M. & Bellamine, A. Trimethylamine N-Oxide in Relation to
864 Cardiometabolic Health-Cause or Effect? *Nutrients* **12**, (2020).
865 78. Zeisel, S. H. Dietary choline: biochemistry, physiology, and pharmacology. *Annu.*
866 *Rev. Nutr.* **1**, 95–121 (1981).
867 79. Lundstrom, R. C. & Racicot, L. D. Gas chromatographic determination of
868 dimethylamine and trimethylamine in seafoods. *J. - Assoc. Off. Anal. Chem.* **66**,
869 1158–1163 (1983).

80. Zeng, L.-F. *et al.* An exploration of the role of a fish-oriented diet in cognitive decline: a systematic review of the literature. *Oncotarget* **8**, 39877–39895 (2017).
81. Keenan, T. D. *et al.* Adherence to a Mediterranean diet and cognitive function in the Age-Related Eye Disease Studies 1 & 2. *Alzheimers Dement.* **16**, 831–842 (2020).
82. Zhao, W. *et al.* Fish Consumption and Stroke Risk: A Meta-Analysis of Prospective Cohort Studies. *J. Stroke Cerebrovasc. Dis. Off. J. Natl. Stroke Assoc.* **28**, 604–611 (2019).
83. Zhang, Y. *et al.* Intakes of fish and polyunsaturated fatty acids and mild-to-severe cognitive impairment risks: a dose-response meta-analysis of 21 cohort studies. *Am. J. Clin. Nutr.* **103**, 330–340 (2016).
84. Cooper, R. E., Tye, C., Kuntsi, J., Vassos, E. & Asherson, P. Omega-3 polyunsaturated fatty acid supplementation and cognition: A systematic review and meta-analysis. *J. Psychopharmacol. Oxf. Engl.* **29**, 753–763 (2015).
85. Abdelhamid, A. S. *et al.* Omega-3 fatty acids for the primary and secondary prevention of cardiovascular disease. *Cochrane Database Syst. Rev.* **11**, CD003177 (2018).
86. Gobbetti, T. & Cooray, S. N. Annexin A1 and resolution of inflammation: tissue repairing properties and signalling signature. *Biol. Chem.* **397**, 981–993 (2016).
87. Wall, R., Ross, R. P., Fitzgerald, G. F. & Stanton, C. Fatty acids from fish: the anti-inflammatory potential of long-chain omega-3 fatty acids. *Nutr. Rev.* **68**, 280–289 (2010).
88. Nicholson, J. K. *et al.* Host-gut microbiota metabolic interactions. *Science* **336**, 1262–7 (2012).
89. Needham, B. D., Kaddurah-Daouk, R. & Mazmanian, S. K. Gut microbial molecules in behavioural and neurodegenerative conditions. *Nat. Rev. Neurosci.* **21**, 717–731 (2020).

898 **Table 1.** BBB-associated genes whose expression was upregulated upon exposure
899 of hCMEC/D3 cells to TMAO.
900

Gene	Entrez ID	Description	Log_2 fold change	Category	P_{FDR}
TFRC	7037	Transferrin receptor	0.23	Transporter proteins	0.054
ABCC4	10257	ATP binding cassette subfamily C member 4	0.20	Transporter proteins	0.088
ANXA1	301	Annexin A1	0.16	Cell Adhesion/Junctional proteins/Cytoskeletal factors	0.088
CDH2	1000	Cadherin 2	0.31	Cell Adhesion/Junctional proteins/Cytoskeletal factors	0.095

901
902
903

904 **Table 2.** Daily consumption of TMAO and water in mice chronically treated with TMAO
905 and/or LPS.
906
907 Data are mean ± standard deviation.
908

Variable	Sham-treated mice	LPS-treated mice	*P* value
TMAO intake (mg/day/mouse)	2.79 ± 0.38	2.82 ± 0.25	0.7
TMAO intake (mg/kg/mouse)	85.0 ± 11.4	88.9 ± 7.9	0.14
Water consumption (ml/day/mouse)	5.57 ± 0.8	5.64 ± 0.5	0.48

909
910
911
912

913 **FIGURE LEGENDS**

914 **Fig. 1.** Effects of TMAO and TMA on integrity of hCMEC/D3 cell monolayers. (A)
915 Assessment of paracellular permeability of hCMEC/D3 monolayers to a 70 kDa FITC-
916 dextran tracer following treatment for 24 h with varying doses of TMA (0.4 – 40 μM) or
917 TMAO (40 – 4000 μM). Data are expressed as mean ± s.e.m., *n*=4 independent
918 experiments. (B) Assessment of TEER of hCMEC/D3 monolayers to a 70kDa FITC-
919 dextran tracer following treatment for 24 h with varying doses of TMA (0.4 – 40 μM) or
920 TMAO (40 – 4000 μM). Data are expressed as mean ± s.e.m., *n*=4 independent
921 experiments. (C) Adhesion of U937 monocytic cells to TNFα-stimulated hCMEC/D3
922 monolayers (10 ng/ml, 16 h) that had been treated or not for 24 h with 0.4 μM TMA or
923 40 μM TMAO. Data are expressed as mean ± s.e.m., *n*=3 independent experiments.
924

925 **Fig. 2.** Effects of TMA and TMAO on gene expression in hCMEC/D3 cells. (A)
926 Heatmap showing expression of the 49 genes found to be significantly (P_{FDR}<0.1)
927 differentially expressed upon exposure of hCMEC/D3 cells to 0.4 μM TMA (*n*=5 per
928 group). (B) Heatmap showing expression of the 440 genes found to be significantly
929 (P_{FDR}<0.1) differentially expressed upon exposure of hCMEC/D3 cells to 40 μM TMAO
930 (*n*=5 per group). (C) Biological processes associated with genes found to be
931 significantly upregulated (*n*=39) or downregulated (*n*=10) upon exposure of cells to
932 TMA. (D) Biological processes of genes found to be significantly upregulated (*n*=341)
933 or downregulated (*n*=99) upon exposure of cells to TMAO. Images in (C, D) shown
934 based on Enrichr *P* value ranking from GO analysis. (E) Topological analysis of the
935 KEGG networks associated with the 440 genes whose expression was significantly
936 affected upon exposure of cells to TMAO (blue, significantly downregulated; red,
937 significantly upregulated); genes of similar cellullar role are highlighted. (F) Confocal
938 microscopic analysis of expression of fibrillar actin (F-actin) and the tight junction
939 component zonula occludens-1 (ZO-1) in hCMEC/D3 cells following treatment for 24
940 h with 0.4 μM TMA or 40 μM TMAO. Images are representative of at least three
941 independent experiments.
942

943 **Fig. 3.** Annexin A1 (ANXA1) signalling mediates effects of TMAO on hCMEC/D3 cells.
944 (A) Total cellular expression of ANXA1 in hCMEC/D3 cells treated for 24 h with 0.4
945 μM TMA or 40 μM TMAO. Data are expressed as mean ± s.e.m., *n*=5-7 independent

946 experiments. (B) Medium ANXA1 content of hCMEC/D3 monolayers treated for 24 h
947 with 0.4 μM TMA or 40 μM TMAO. Data are expressed as mean ± s.e.m., *n*=3
948 independent experiments. (C) Assessment of paracellular permeability of monolayers
949 of wild-type hCMEC/D3 cells, or hCMEC/D3 cells stably transfected with either a
950 scramble shRNA sequence or an shRNA sequence targeting ANXA1 to a 70kDa FITC-
951 dextran tracer following treatment for 24 h with 40 μM TMAO. Data are expressed as
952 mean ± s.e.m., *n*=4 independent experiments. (D) Assessment of TEER of
953 monolayers of wild-type hCMEC/D3 cells, or hCMEC/D3 cells stably transfected with
954 either a scramble shRNA sequence or an shRNA sequence targeting ANXA1 following
955 treatment for 24 h with 40 μM TMAO. Data are expressed as mean ± s.e.m., *n*=4
956 independent experiments. (E) Assessment of paracellular permeability of hCMEC/D3
957 cells to a 70kDa FITC-dextran tracer following treatment for 24 h with 40 μM TMAO,
958 with or without 10 min pre-treatment with the FPR2 antagonist WRW_4 (10 μM). Data
959 are expressed as mean ± s.e.m., *n*=3 independent experiments. (F) Assessment of
960 TEER of hCMEC/D3 cells following treatment for 24 h with 40 μM TMAO, with or
961 without 10 min pre-treatment with the FPR2 antagonist WRW4 (10 μM). Data are
962 expressed as mean ± s.e.m., *n*=3 independent experiments.
963
964 **Fig. 4.** Acute treatment with TMAO promotes BBB integrity *in vivo*. (A) Extravasation
965 of Evans blue dye into brain parenchyma over a 1 h period in 2-month-old male
966 C57Bl/6J mice following i.p. injection of 1.8 mg/kg TMAO for 2 h, 6 h or 24 h *vs.* a
967 saline injected control. Data are normalised to plasma Evans blue content, and are
968 expressed as mean ± s.e.m., *n*=5-6 mice. (B) Extravasation of Evans blue dye into
969 brain parenchyma over a 1 h period in 2-month-old male C57Bl/6J mice following i.p.
970 injection of saline or E. coli O111:B4 LPS (3 mg/kg) with or without subsequent i.p.
971 injection of 1.8 mg/kg TMAO according to the schedule shown. Data are normalised
972 to plasma Evans blue content, and are expressed as mean ± s.e.m., *n*=4-6 mice.
973
974 **Fig. 5.** Acute exposure of mice to TMAO significantly alters the whole brain
975 transcriptome. (A) Heatmap showing expression of the 76 genes found to be
976 significantly (P_{FDR}<0.1) differentially expressed in the mouse brain after 2 h exposure
977 to 1.8 mg/kg TMAO (*n*=3 per group). Data were scaled by row. (B) Over-representation
978 analysis (Enrichr) showing KEGG pathways associated with the 76 genes. (C)

979 Comparative analysis of significantly differentially expressed genes identified
980 groupings associated with distinct biological functions. (D) Among the 197 BBB-
981 specific genes identified in the data set, only *App* and *Cpe* were significantly
982 (P_{FDR}<0.1) differentially expressed in the mouse brain after 2 h exposure to TMAO.
983 Data are shown as mean ± s.d, *n*=3 per group. Individual data points are not shown
984 due to the negligible values of the s.d.
985
986 **Fig. 6.** Effect of long-term TMAO exposure on BBB integrity and cognitive function of
987 mice. (A) Body weight gain in mice treated with TMAO through their drinking water
988 (0.5 mg/ml) over 2 months, combined with a chronic low dose administration of LPS
989 (0.5 mg/kg/week, i.p.). Data are expressed as mean ± s.e.m., *n*=8 mice, columns with
990 different letters are significantly different at *P*<0.05. (B) Cerebellar permeability index
991 to sodium fluorescein 2h following administration in animals previously treated with
992 TMAO through their drinking water (0.5 mg/ml) over 2 months, combined with a
993 chronic low dose administration of LPS (0.5 mg/kg/week, i.p.). Data are expressed as
994 mean ± s.e.m., *n*=8 mice, columns with different letters are significantly different at
995 *P*<0.05. (C) Typical confocal microscopic images of perivascular IgG deposition in
996 male C57Bl/6J mice treated with TMAO through their drinking water (0.5 mg/ml) over
997 2 months, combined with a chronic low dose administration of LPS (0.5 mg/kg/week,
998 i.p.). *Griffonia simplicifolia* isolectin B_4 (red) defines endothelial cells, areas of IgG
999 deposition (white) are highlighted by arrow heads. (D) Distance travelled, (E)
1000 movement speed and (F) percentage of time in the centre as measured in the OFT in
1001 animals previously treated with TMAO through their drinking water (0.5 mg/ml) over 2
1002 months, combined with a chronic low dose administration of LPS (0.5 mg/kg/week,
1003 i.p.). Data are expressed as mean ± s.e.m., *n*=8 mice. (G) Novel object discrimination
1004 index, calculated as described in Methods, of animals previously treated with TMAO
1005 through their drinking water (0.5 mg/ml) over 2 months, combined with a chronic low
1006 dose administration of LPS (0.5 mg/kg/week, i.p.). Data are expressed as mean ±
1007 s.e.m., *n*=8 mice, columns with different letters are significantly different at *P*<0.05.
1008 (H) Percentage of spontaneous alternation and (I) total distance travelled in the Y-
1009 maze test for animals previously treated with TMAO through their drinking water (0.5
1010 mg/ml) over 2 months, combined with a chronic low dose administration of LPS (0.5
1011 mg/kg/week, i.p.). Data are expressed as mean ± s.e.m., *n*=8 mice.
1012

1013 **Supplementary Fig. 1.** Confirmation of ANXA1 targeting and knock-down in
1014 hCMEC/D3 cells stably transfected with appropriate shRNA sequences. (A) Typical
1015 flow cytometric profiles of wild-type cells, cells transfected with a scramble shRNA
1016 sequence and cells transfected with an ANXA1-targeting shRNA sequence, alongside
1017 unstained and second antibody controls. (B) Expression of ANXA1 in wild-type
1018 hCMEC/D3 cells, cells transfected with a scramble shRNA sequence and cells
1019 transfected with an ANXA1-targeting shRNA sequence. Data are expressed as mean
1020 ± s.e.m., *n*=4 independent experiments.
1021
1022 **Supplementary Fig. 2.** Neither TMAO nor TMA treatment affected the major
1023 endothelial efflux transporters BCRP or P-glycoprotein. (A-D) *In vitro* analysis revealed
1024 no significant effects of either TMAO or TMA upon BCRP (A, C) or P-glycoprotein (B,
1025 D) activity. Dashed lines represent Loess regression fits, with shading representing
1026 95% confidence intervals. (E) hCMEC/D3 cell surface expression of BCRP was
1027 unaffected by 24 h exposure to TMA (0.4 μM) or TMAO (40 μM). Data are expressed
1028 as mean ± s.e.m., *n*=3 independent experiments. (F) hCMEC/D3 cell surface
1029 expression of P-glycoprotein was unaffected by 24 h exposure to TMA (0.4 μM) or
1030 TMAO (40 μM). Data are expressed as mean ± s.e.m., *n*=3 independent experiments.
1031
1032 **Supplementary Fig. 3.** *In vitro* (hCMEC/D3 cell) *FMO3* gene expression is unaffected
1033 by exposure to TMA (0.4 μM) or TMAO (40 μM). Dark blue lines represent the standard
1034 deviation (+/-). There was no statistically significant difference between TMA and the
1035 control, nor between TMAO and the control (Supplementary Tables 2 and 3).
1036 Individual data points are not shown due to the negligible values of the standard
1037 deviations.
1038
1039 **Supplementary Fig. 4.** Neither chronic low-dose LPS nor TMAO treatment
1040 significantly increases serum inflammatory cytokines. (A) Serum TNFα concentrations
1041 in male C57Bl/6J mice treated with TMAO through their drinking water (0.5 mg/ml)
1042 over 2 months, combined with a chronic low dose administration of LPS (0.5
1043 mg/kg/week, i.p.). Data are expressed as mean ± s.e.m., *n*=7-8 mice. (B) Serum IL-
1044 1β concentrations in male C57Bl/6J mice treated with TMAO through their drinking
1045 water (0.5 mg/ml) over 2 months, combined with a chronic low dose administration of

1046 LPS (0.5 mg/kg/week, i.p.). Data are expressed as mean ± s.e.m., *n*=7-8 mice.
1047
1048 **Supplementary Table 1.** Normalized microarray data for hCMEC/D3 treated or not
1049 with TMA (0.4 μM) or TMAO (40 μM)
1050
1051 **Supplementary Table 2.** Differential gene expression for control compared with TMA
1052 treatment, as assessed using LIMMA
1053
1054 **Supplementary Table 3.** Differential gene expression for control compared with
1055 TMAO treatment, as assessed using LIMMA
1056
1057 **Supplementary Table 4.** KEGG-based SPIA of genes whose expression was
1058 significantly affected by TMAO
1059
1060 **Supplementary Table 5.** GO (biological process) analysis of TMA-up-regulated
1061 genes as assessed using Enrichr
1062
1063 **Supplementary Table 6.** GO (biological process) analysis of TMA-down-regulated
1064 genes as assessed using Enrichr
1065
1066 **Supplementary Table 7.** GO (biological process) analysis of TMAO-up-regulated
1067 genes as assessed using Enrichr
1068
1069 **Supplementary Table 8.** GO (biological process) analysis of TMAO-down-regulated
1070 genes as assessed using Enrichr
1071
1072 **Supplementary Table 9.** Differential gene expression of BBB-associated genes (*in*
1073 *vitro* TMA treatment)
1074
1075 **Supplementary Table 10.** Differential gene expression of BBB-associated genes (*in*
1076 *vitro* TMAO treatment)
1077

1078 **Supplementary Table 11.** Differential gene expression in mouse brain for control
1079 compared with TMAO treatment, as assessed using DESeq2
1080
1081 **Supplementary Table 12.** Differential expression of BBB-associated genes in mouse
1082 brain for control compared with TMAO treatment, as assessed using DESeq2
1083

Figure 1

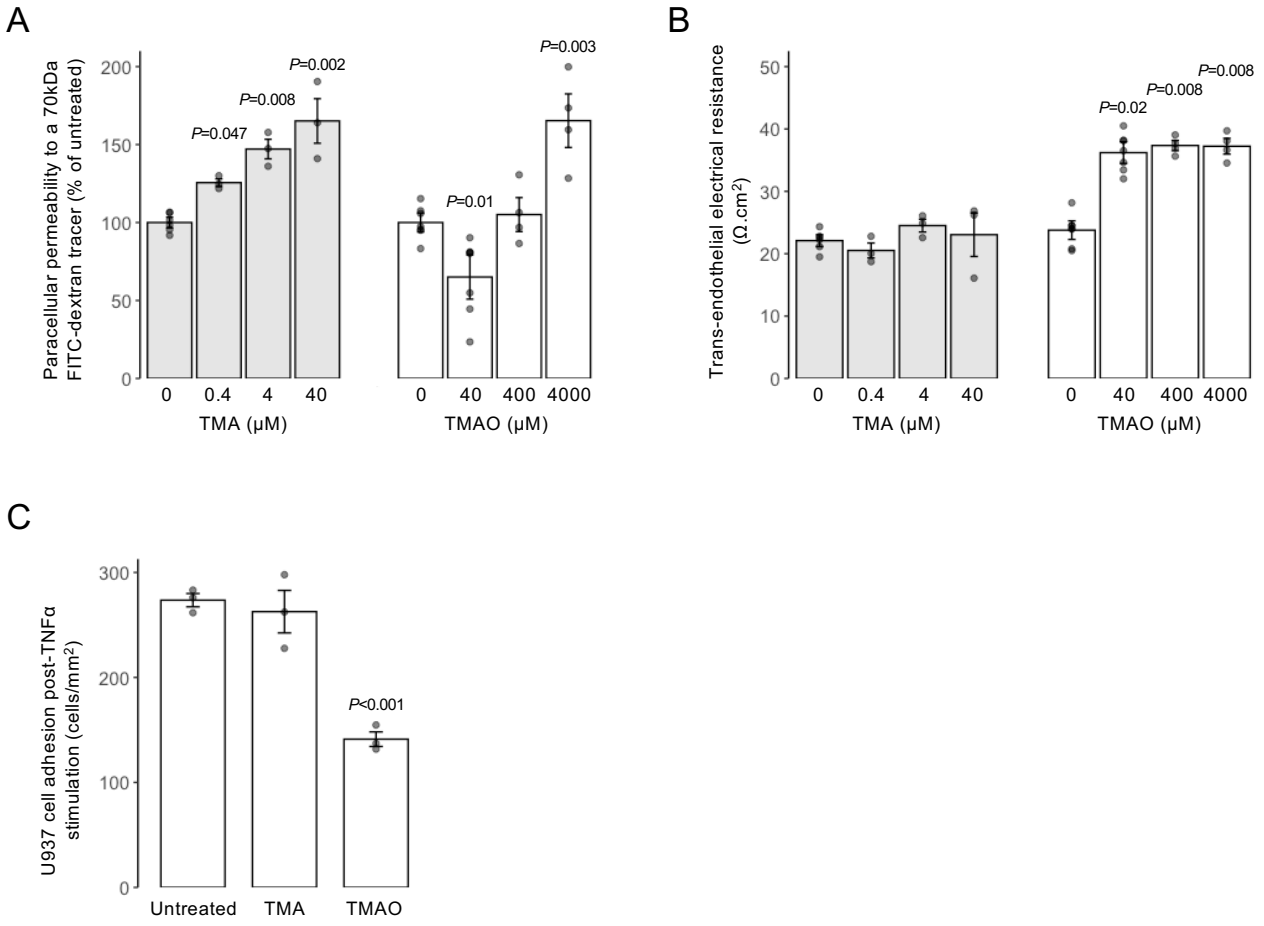
A
Paracellular permeability to a 70kDa FITC-dextran tracer (% of untreated)
200
150
100
50
0
P=0.047
P=0.008
P=0.002
P=0.01
P=0.003
0
0.4
4
40
TMA (µM)
0
40
400
4000
TMAO (µM)
B
Trans-endothelial electrical resistance (Ω.cm²)
50
40
30
20
10
0
P=0.02
P=0.008
P=0.008
0
0.4
4
40
TMA (µM)
0
40
400
4000
TMAO (µM)
C
U937 cell adhesion post-TNFα stimulation (cells/mm²)
300
200
100
0
P<0.001
Untreated
TMA
TMAO

Figure 2

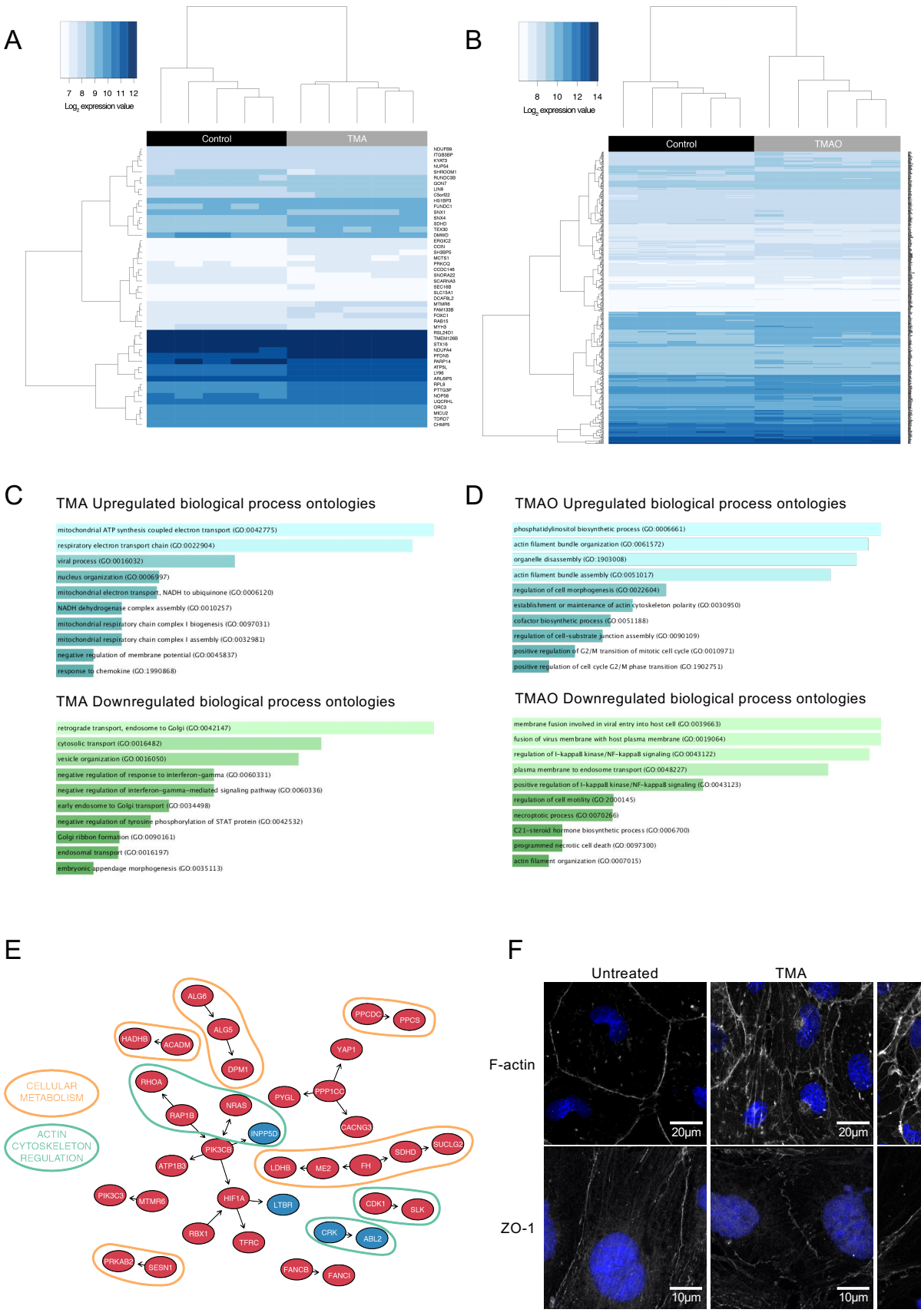
A
7 8 9 10 11 12
Log2 expression value
Control
TMA
B
8 10 12 14
Log2 expression value
Control
TMAO
C
TMA Upregulated biological process ontologies
mitochondrial ATP synthesis coupled electron transport (GO:0042775)
respiratory electron transport chain (GO:0022904)
viral process (GO:0016032)
nucleus organization (GO:0006997)
mitochondrial electron transport, NADH to ubiquinone (GO:0006120)
NADH dehydrogenase complex assembly (GO:0010257)
mitochondrial respiratory chain complex I biogenesis (GO:0097031)
mitochondrial respiratory chain complex I assembly (GO:0032981)
negative regulation of membrane potential (GO:0045837)
response to chemokine (GO:1990868)
TMA Downregulated biological process ontologies
retrograde transport, endosome to Golgi (GO:0042147)
cytosolic transport (GO:0016482)
vesicle organization (GO:0016050)
negative regulation of response to interferon-gamma (GO:0060331)
negative regulation of interferon-gamma-mediated signaling pathway (GO:0060336)
early endosome to Golgi transport (GO:0034498)
negative regulation of tyrosine phosphorylation of STAT protein (GO:0042532)
Golgi ribbon formation (GO:0090161)
endosomal transport (GO:0016197)
embryonic appendage morphogenesis (GO:0035113)
D
TMAO Upregulated biological process ontologies
phosphatidylinositol biosynthetic process (GO:0006661)
actin filament bundle organization (GO:0061572)
organelle disassembly (GO:1903008)
actin filament bundle assembly (GO:0051017)
regulation of cell morphogenesis (GO:0022604)
establishment or maintenance of actin cytoskeleton polarity (GO:0030950)
cofactor biosynthetic process (GO:0051188)
regulation of cell-substrate junction assembly (GO:0090109)
positive regulation of G2/M transition of mitotic cell cycle (GO:0010971)
positive regulation of cell cycle G2/M phase transition (GO:1902751)
TMAO Downregulated biological process ontologies
membrane fusion involved in viral entry into host cell (GO:0039663)
fusion of virus membrane with host plasma membrane (GO:0019064)
regulation of I-kappaB kinase/NF-kappaB signaling (GO:0043122)
plasma membrane to endosome transport (GO:0048227)
positive regulation of I-kappaB kinase/NF-kappaB signaling (GO:0043123)
regulation of cell motility (GO:2000145)
necroptotic process (GO:0070266)
C21-steroid hormone biosynthetic process (GO:0006700)
programmed necrotic cell death (GO:0097300)
actin filament organization (GO:0007015)
E
CELLULAR METABOLISM
ACTIN CYTOSKELETON REGULATION
ALG6
ALG5
DPM1
HADHB
ACADM
PPCDC
PPCS
YAP1
RHOA
RAP1B
NRAS
PYGL
PPP1CC
CACNG5
INPP5D
PIK3CB
ATP1B3
SDHD
SUCLG2
LDHB
ME2
FH
PIK3C3
MTMR6
HIF1A
LTBR
CDK1
SLK
RBX1
TFRC
CRK
ABL2
PRKAB2
SESN1
FANCB
FANCI
F
Untreated
TMA
TMAO
F-actin
ZO-1
20μm
10μm

Figure 3

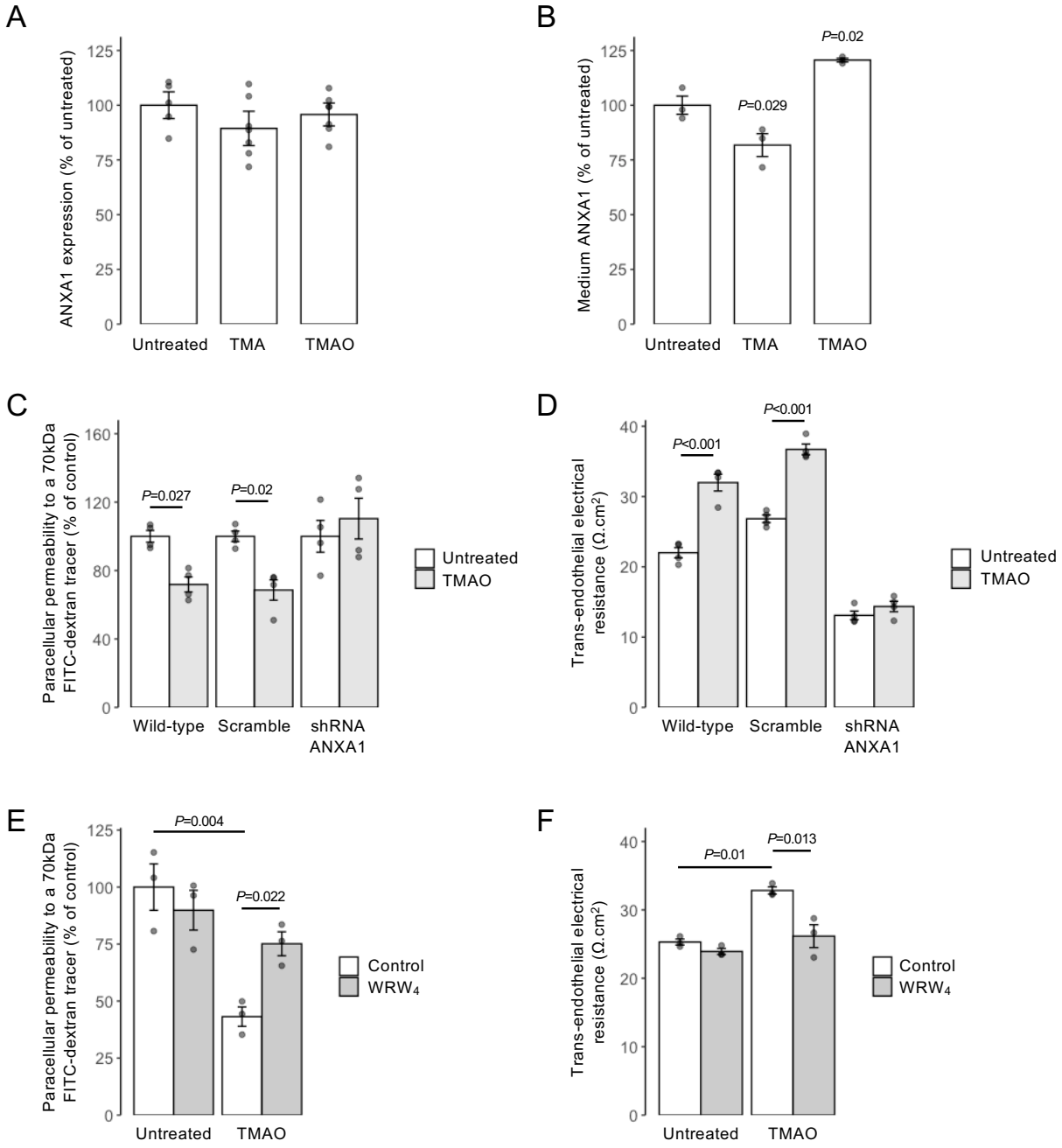
A
ANXA1 expression (% of untreated)
125
100
75
50
25
0
Untreated
TMA
TMAO
B
Medium ANXA1 (% of untreated)
P=0.02
P=0.029
Untreated
TMA
TMAO
C
Paracellular permeability to a 70kDa FITC-dextran tracer (% of control)
160
120
80
40
0
P=0.027
P=0.02
Wild-type
Scramble
shRNA ANXA1
Untreated
TMAO
D
Trans-endothelial electrical resistance (Ω.cm²)
40
30
20
10
0
P<0.001
P<0.001
Wild-type
Scramble
shRNA ANXA1
Untreated
TMAO
E
Paracellular permeability to a 70kDa FITC-dextran tracer (% of control)
P=0.004
P=0.022
Untreated
TMAO
Control
WRW4
F
Trans-endothelial electrical resistance (Ω.cm²)
P=0.01
P=0.013
Untreated
TMAO
Control
WRW4

Figure 4

A

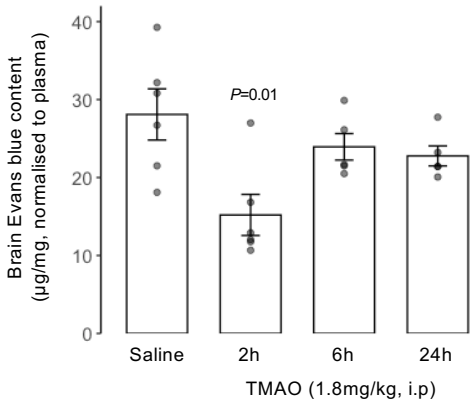
Brain Evans blue content
(µg/mg, normalised to plasma)
40
30
20
10
0
P=0.01
Saline
2h
6h
24h
TMAO (1.8mg/kg, i.p)

B

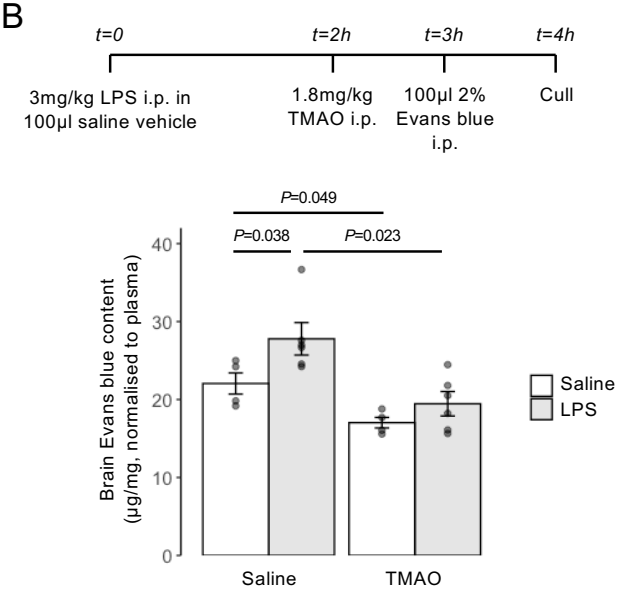
t=0
t=2h
t=3h
t=4h
3mg/kg LPS i.p. in
100µl saline vehicle
1.8mg/kg
TMAO i.p.
100µl 2%
Evans blue
i.p.
Cull
P=0.049
P=0.038
P=0.023
Brain Evans blue content
(µg/mg, normalised to plasma)
40
30
20
10
0
Saline
TMAO
Saline
LPS

Figure 5

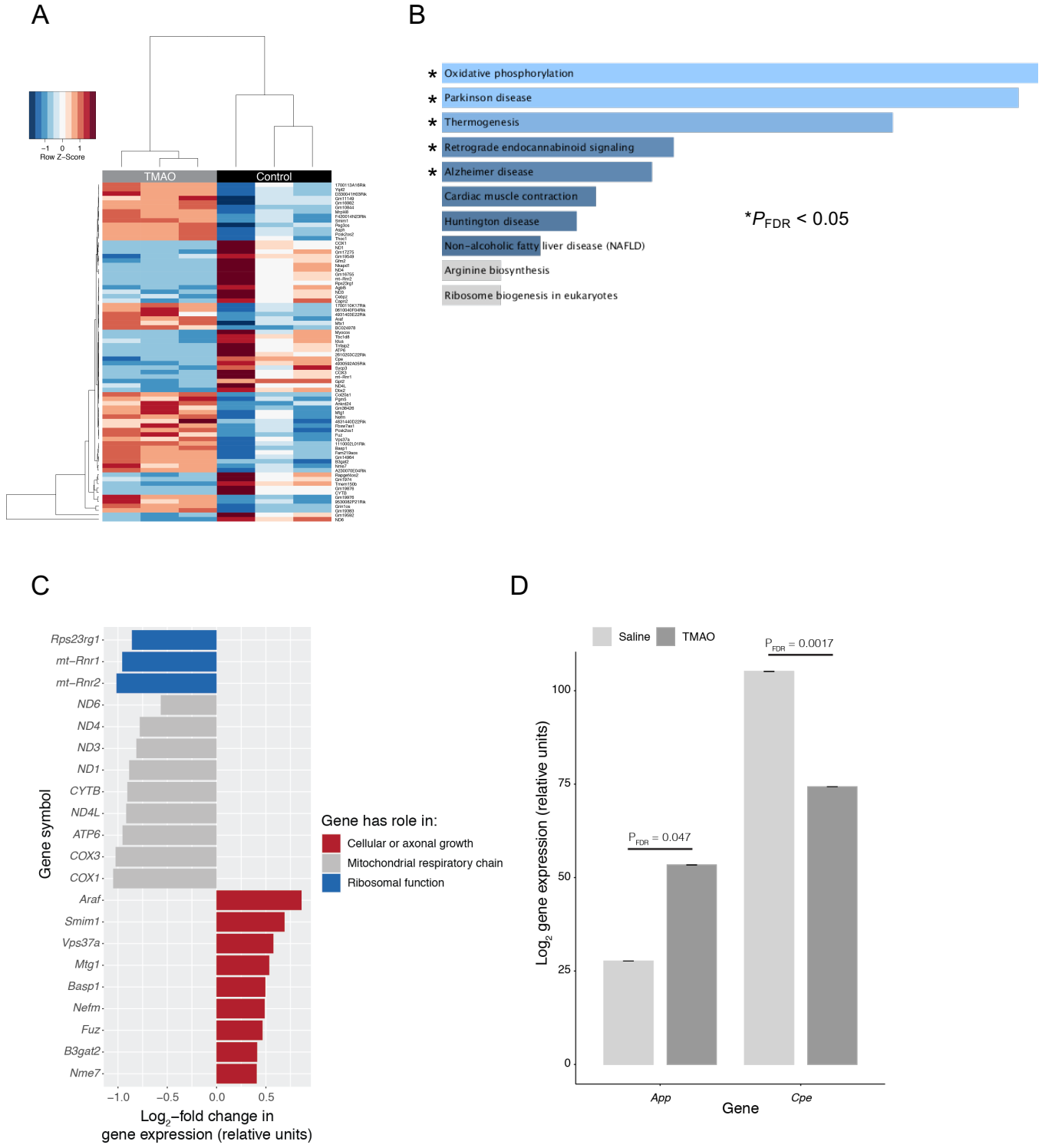
A
−1 0 1
Row Z-Score
TMAO
Control
B
Oxidative phosphorylation
Parkinson disease
Thermogenesis
Retrograde endocannabinoid signaling
Alzheimer disease
Cardiac muscle contraction
Huntington disease
Non-alcoholic fatty liver disease (NAFLD)
Arginine biosynthesis
Ribosome biogenesis in eukaryotes
*P_FDR < 0.05
C
Rps23rg1
mt−Rnr1
mt−Rnr2
ND6
ND4
ND3
ND1
CYTB
ND4L
ATP6
COX3
COX1
Araf
Smim1
Vps37a
Mtg1
Basp1
Nefm
Fuz
B3gat2
Nme7
Gene symbol
−1.0 −0.5 0.0 0.5
Log2−fold change in gene expression (relative units)
Gene has role in:
Cellular or axonal growth
Mitochondrial respiratory chain
Ribosomal function
D
Saline
TMAO
P_FDR = 0.0017
P_FDR = 0.047
Log2 gene expression (relative units)
0 25 50 75 100
App
Cpe
Gene

Figure 6

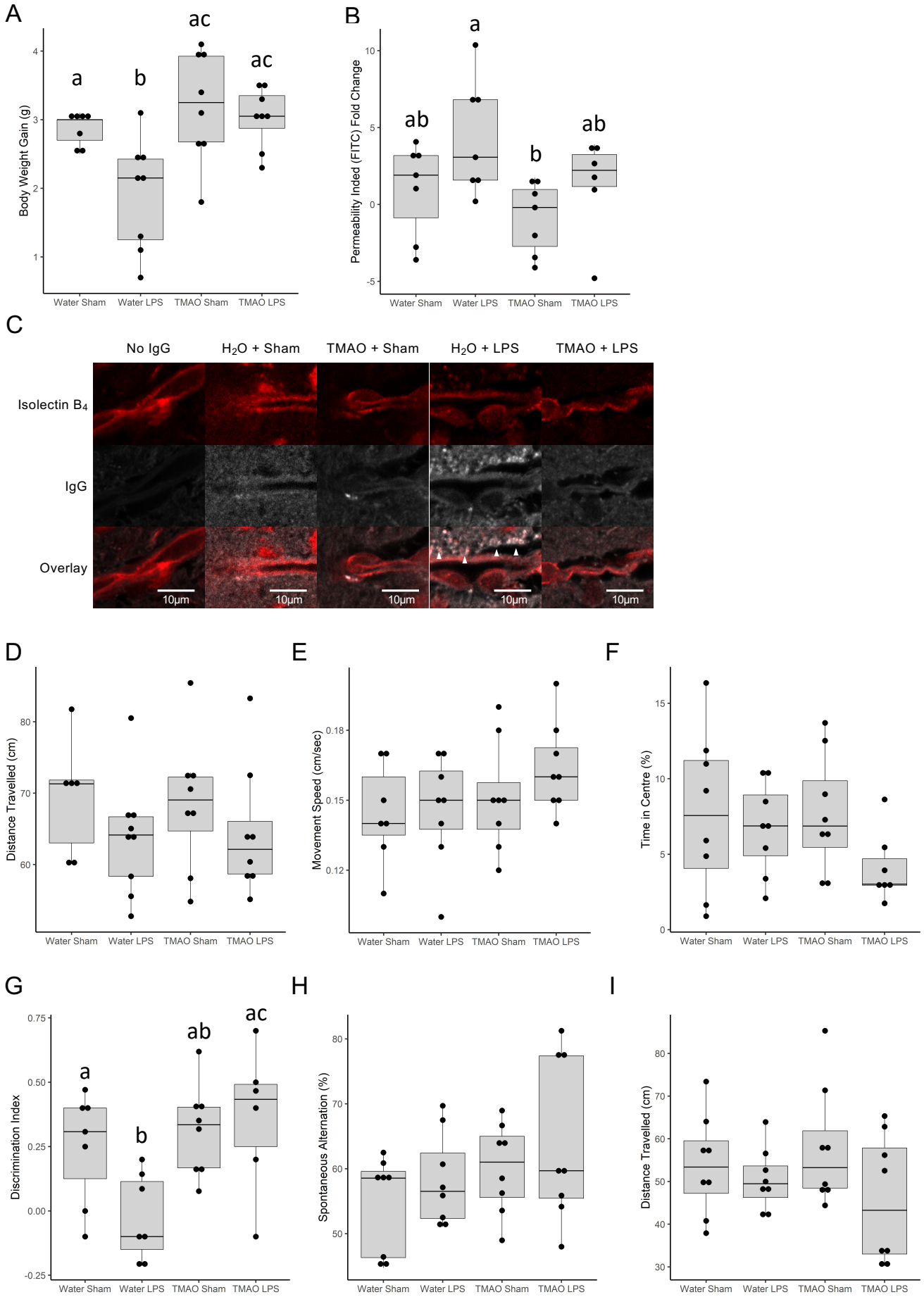
A
Body Weight Gain (g)
a
b
ac
ac
Water Sham
Water LPS
TMAO Sham
TMAO LPS
B
Permeability Inded (FITC) Fold Change
ab
a
b
ab
C
No IgG
H2O + Sham
TMAO + Sham
H2O + LPS
TMAO + LPS
Isolectin B4
IgG
Overlay
10μm
D
Distance Travelled (cm)
E
Movement Speed (cm/sec)
F
Time in Centre (%)
G
Discrimination Index
a
b
ab
ac
H
Spontaneous Alternation (%)
I
Distance Travelled (cm)

Supplementary Figure 1

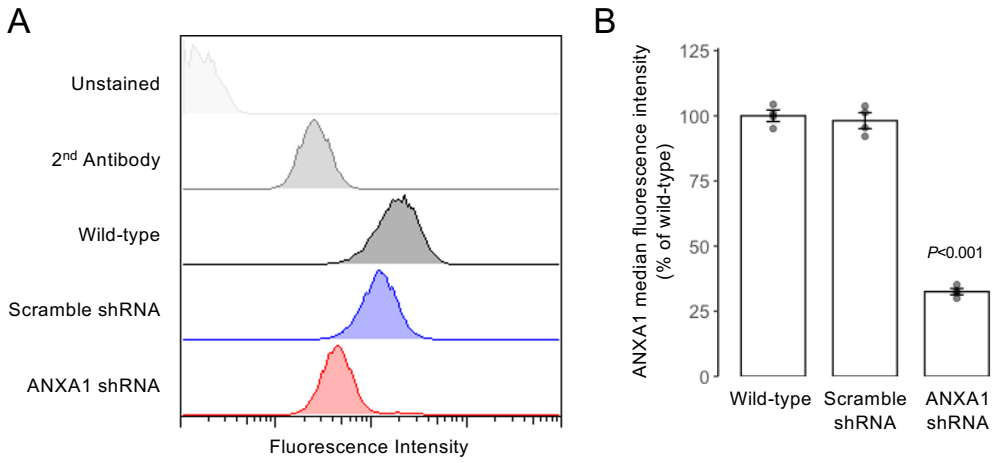

Supplementary Figure 2

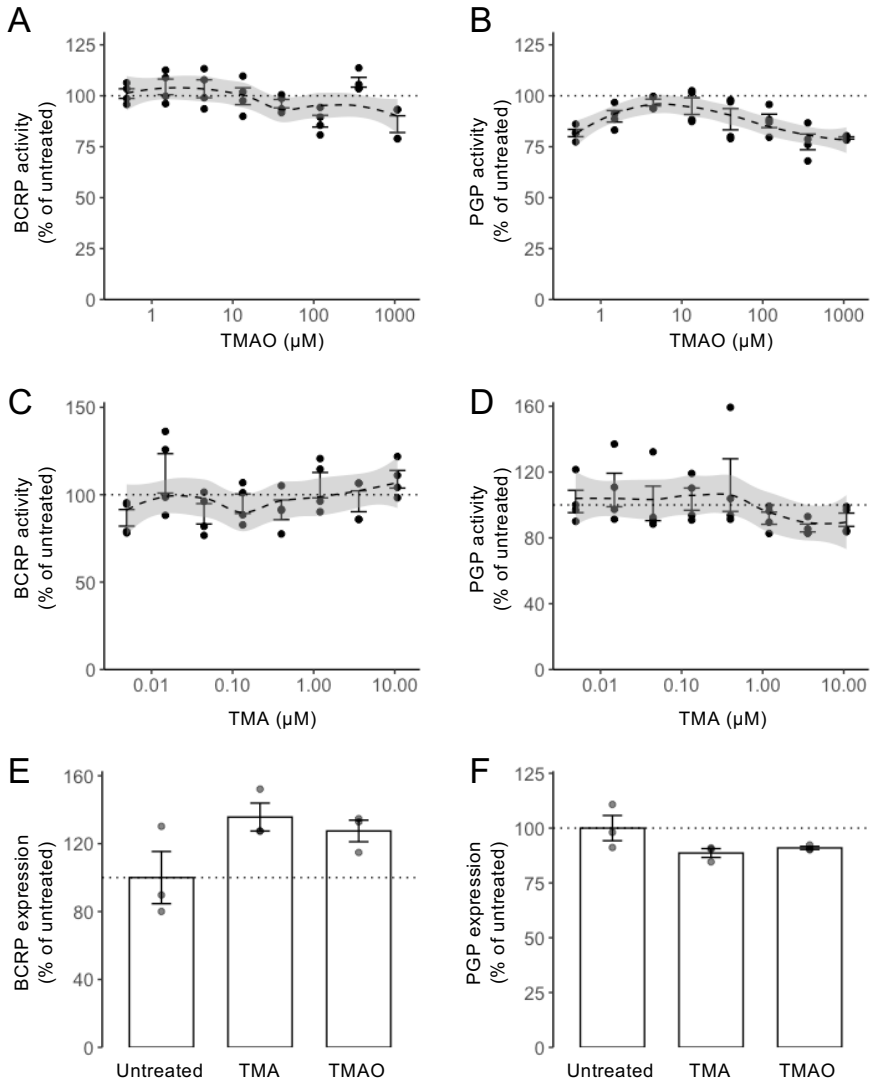

Supplementary Figure 3

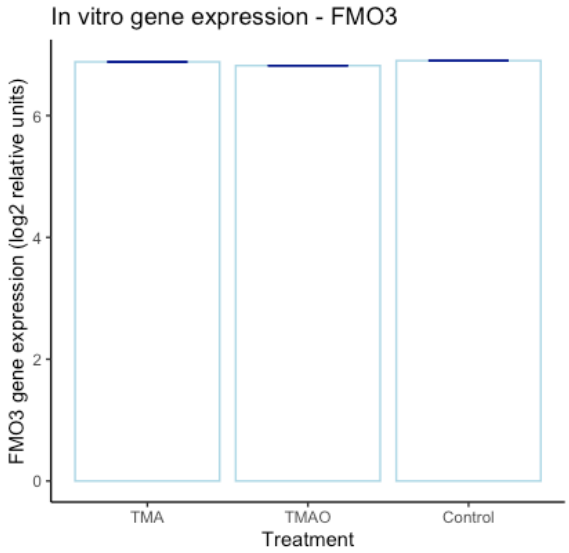
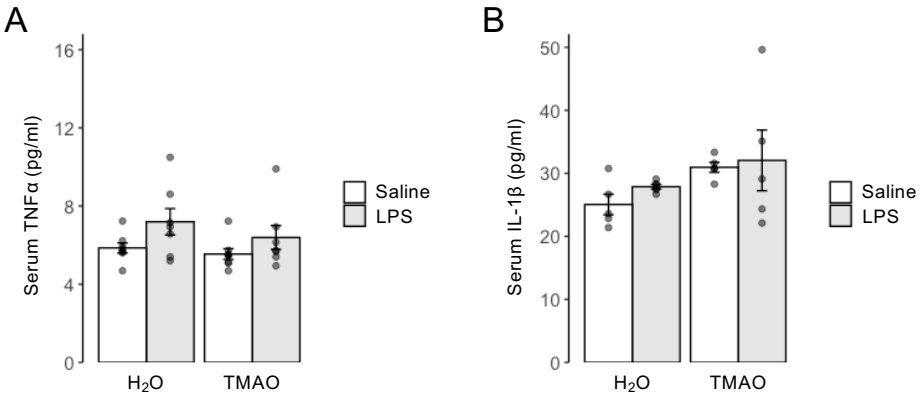
Supplementary Figure 4